Pre-eruptive conditions and dynamics recorded in banded pumices from the El Abrigo caldera-forming eruption (Tenerife, Canary Islands)

Diego González-García[1,2*], Maurizio Petrelli[3], Diego Perugini[3], Daniele Giordano[1], Jérémie Vasseur[4], Joali Paredes-Mariño[3,5], Joan Marti[6], Donald B. Dingwell[4]

[1] Dipartimento di Scienze della Terra, Università degli Studi di Torino, Via Valperga Caluso 35, 10135 Turin, Italy.

[2] Institut für Mineralogie, Leibniz Universität Hannover, Callinstrasse 3, 30167 Hannover, Germany

[3] Dipartimento di Fisica e Geologia, Università degli Studi di Perugia, Piazza Università 1, 06123 Perugia, Italy

[4] Department für Geo- und Umweltwischenchaften, Ludwig-Maximilians Universität München. Theresienstrasse 41, 80333 Munich, Germany

[5] School of Environment, The University of Auckland, Private Bag 92019, Auckland 1142, New Zealand

[6] Geosciences Barcelona (GEO3BCN-CSIC), C/ Lluis Solé i Sabarís, s/n, 08028 Barcelona, Spain

*Corresponding author**:** Diego González-García e-mail: d.gonzalez@mineralogie.uni-hannover.de Telephone: +49 511 762 5676

ABSTRACT

The El Abrigo member of the Diego Hernández Formation (Tenerife, Canary Islands) represents the final (170 ka) and most voluminous eruption (>20 km^3 DRE) of the last cycle of explosive activity of the Las Cañadas volcano. It is a dominantly phonolitic ignimbrite containing both mafic and banded pumices, suggesting that magma mixing played an important role in triggering the eruption and modulating eruptive dynamics. Here we use petrology, together with glass and mineral geochemistry of enclave-rich mafic scoriae, banded and phonolitic pumices from El Abrigo ignimbrite, to shed light on the pre-eruptive storage conditions and processes governing magma ascent and interaction dynamics and to provide a first-order assessment of the contribution of magma mixing and crystal mush melting to the dynamics of this eruptive event. The distribution of major elements in glasses is consistent with diffusive exchange between the interacting melts whereby Na transfers from the phonolite to the tephriphonolitic melt. However, V, Zr, Ba and Eu suggest a complex scenario in which an intruding tephritic to phonotephritic magma interacted with two distinct zones of a phonolitic magma chamber, one occupied by a crystal rich, low-Zr and high Ba phonolite, and the other by an evolved, crystal poor, high-Zr phonolite. These results, coupled with mineral-melt thermobarometry, allow us to reconstruct the Las Cañadas plumbing system at the end of the Diego Hernández cycle, and to evaluate the contribution of cumulate mush melting and magma mixing in as follows: (1) the parental tephritic magma was stored at or near the Moho (410-450 MPa) at 1050ºC where it was periodically replenished by more primitive basanitic magma; (2) upon ascent, the tephrite intruded into a shallow and zoned phonolitic storage system, triggering the disruption of a crystal mush in its base,

and (3) subsequently interacted with a crystal-poor zone within the reservoir. Energy balance evaluations suggest that relative mafic volume ratios ranged between 20 and 43 vol %, and the conservation of small-scale magma mingling structures and their geochemical distribution suggest that the mixing event took place very shortly before the eruption, on a timescale of hours.

Key words: magma mixing, mush, ignimbrite, banded pumice, trace elements, volcanic glass, phonolite

INTRODUCTION

The study of volcanic plumbing systems in ocean island volcanoes offers an opportunity to explore the generation and evolution of magmas in an intraplate, thin-crust scenario, potentially exposing petrological processes that are obscured in other geological settings. In such settings, low-degree partial melting of the mantle, followed by differentiation within the crust and island edifice is typically argued to explain their compositional diversity (e.g., Beier et al., 2006, Stroncik et al., 2009), which commonly exhibits a bimodal distribution. Ocean islands show a wide diversity in eruptive style and compositions (Jeffery & Gertisser, 2018), and in several cases large volumes of felsic, peralkaline magmas have been documented in the form of extensive, zoned ignimbritic sheets resulting from highly explosive eruptions (e.g., Freundt & Schminke, 1992; Gertisser et al., 2010). Some of these ignimbrites exhibit a bimodal character, with mafic and felsic end-members, suggesting that the periodical interaction between primitive,

mafic magmas, and shallow crustal, silicic magmas is a recurrent phenomenon (Daly, 1925; Clague, 1978; Jeffery & Gertisser, 2018; Laeger et al., 2019).

Following the discovery of such large bimodal ignimbritic sheets, both in oceanic and continental contexts, the intrusion and subsequent mingling and mixing of mafic magma in more evolved reservoirs has been widely recognized as a triggering mechanism of explosive eruptions (e.g., Sparks et al., 1977; Wolff, 1985; Leonard et al., 2002; Eichelberger & Izbekov, 2000; Morgavi et al., 2017). In this context, a mafic recharge may lead to the partial melting and remobilization of a silicic crystal mush, inevitably involving heat and volatile transfer (e.g., Bachmann & Bergantz, 2003; Montagna et al., 2015, Sliwinski et al., 2015). This process can also trigger convective overturn of the magma reservoir, leading to enhanced mingling and mixing of the melts (Bain et al., 2013), and, finally, eruption by overpressure (Folch & Martí, 1998). Heterogeneous bubble nucleation in the magma-magma interface may increase the explosive potential (Paredes-Mariño et al., 2017).

The geochemical signature of magma mixing has been found in several explosive eruptions such as the 1975 eruption of Askja (Sparks et al., 1977; Sigurdsson & Sparks, 1981), or the 2011 Eyjafjallajokull eruption in Iceland (e.g., Sigmundsson et al., 2010; Sigmarsson et al., 2011; Laeger et al., 2017), and the 1912 Novarupta-Katmai eruption (Eichelberger & Izbekov, 2000). Although most works tend to focus on subduction or continental intraplate settings (Leonard et al., 2002; Perugini et al., 2003, 2010; Morgavi et al., 2016; Rossi et al., 2019), alkaline ocean island volcanoes have also been the focus of studies on magma mixing (Wolff, 1985; Araña et al., 1994, Freundt & Schminke, 1992; Laeger et al., 2019, Wiesmaier et al., 2011, Chamberlain et al., 2020).

Several examples of compositionally zoned ignimbrites occur in the Diego Hernández Formation (DHF), cropping out in the SE of the island of Tenerife (Canary Islands), where a thick pyroclastic succession, spanning ca. 600 to 170 ka in age, crops out in the SE sector of the island (e.g., Bryan et al., 1998). This succession was generated by the last of three cycles of major explosive eruptions in the Las Cañadas edifice, predating the currently active Teide-Pico Viejo complex (Martí et al., 1994). The El Abrigo member of the DHF is the youngest (170 ka) and most voluminous (>20 km^3 dense rock equivalent, DRE) (Brown et al., 2003; Edgar et al., 2007; Andújar et al., 2008). Although it is dominantly phonolitic, mafic and banded clasts represent a significant fraction of the deposits (between 5% and 40% of the total pumice population; Pittari, 2004). In the past, a number of studies have been carried out on the DHF ignimbrites showing signs of mafic-felsic interaction. However, only a few studies have been carried out on the intra-eruption chemical variability of the erupted products (e.g., Wolff, 1985; Edgar et al., 2002). Unfortunately, these studies do not enable the precise constraining of the influence of pre- and syn-eruptive chemical variability on the dynamics of the eruptive events. In detail, the effects of the reactivation of crystal mushes and cumulates have already been studied in El Abrigo and other units of the DHF (Sliwinski et al., 2015; Wolff et al., 2015; 2020), but the contribution of magma mixing, together with many geochemical aspects of the ignimbrites in the DHF, remain to be investigated in detail and require further research.

The present work provides new insights into the onset and development of the magma mixing event that may have triggered the El Abrigo eruption and the plumbing system leading to such an event. Our main methods are to assess the provenance and properties

of the end-members involved and to use those together with trace element data to shed light on the relative roles of magma mixing and cumulate and/or mush melting in the stages leading up to the eruption. To address this, we have performed a detailed geochemical study of glasses and minerals in a variety of felsic, mafic, and mixed components of the deposit, including novel thermobarometric results for Tenerife. Previous studies have provided data on a variety of products from the El Abrigo ignimbrite, but in the present work we put special emphasis on the small-scale mingling structures present in the mafic to mixed fraction of the juvenile material. In addition, Raman spectroscopy is used to provide information on the in-situ H_2O content of the analysed glasses. We acknowledge that the present-day activity of the island is markedly different from that of the DHF (i.e., dominated by effusive activity), yet a detailed characterization of past eruptive events on Tenerife is of primary importance as it can provide relevant information for future eruptive scenarios. This is particularly true in Tenerife, where the process of magma mixing has been documented in the prehistorical activity of the currently active Teide-Pico Viejo system (e.g., the 1100 AD Montaña Reventada eruption, Araña et al., 1994; Wiesmaier et al., 2011).

GEOLOGICAL SETTING

Tenerife: geological background

The island of Tenerife is the central and largest of the Canary Islands archipelago, 150 km off the north-western African coast. With an oldest dated volcanism age of 11.9 Ma

(Geldmacher et al., 2004; Guillou et al. 2004), the volcanic evolution of Tenerife is a good example of the typical evolutionary path proposed for ocean island volcanoes. The initial shield stage resulted in the construction of a large basaltic complex (11.6-3.95 Ma), represented by the isolated massifs of Anaga, Teno, and Roque del Conde (Gillou et al., 2004; Longpré et al., 2009; Walter et al., 2005; **Fig. 1**). Tenerife is currently in the rejuvenation phase, starting ca. 3.5 Ma ago with the the formation of Las Cañadas edifice, a voluminous shield volcano built over the remnants of the precedent shields (Ancochea et al., 1990; 1999; Huertas et al., 2002). The Las Cañadas activity was characterized by central, explosive phonolitic volcanism coeval with basaltic rift zone eruptions (3.5-0.17 Ma). Finally, the current cycle of activity at Tenerife (0.17 Ma to present) built the active Teide and Pico Viejo (TPV) stratovolcanoes, characterized by mainly effusive phonolitic activity alternating with ubiquitous basaltic eruptions of the rift systems.

Stratigraphically, Las Cañadas edifice can be divided into two distinct groups. The Lower Group consists of mafic to intermediate products ranging in age from 3.5 to 2.2 Ma; this stage was followed by an Upper Group of Quaternary age (1.57-0.17 Ma) involving three cycles of phonolitic explosive eruptions the Ucanca, Guajara, and Diego Hernández formations. Each of these cycles ended with a major caldera-forming eruption at 1.02, 0.57, and 0.17 Ma respectively (Martí et al., 1994; 1997; Martí & Gundmundsson, 2000). They were possibly linked to the triggering of major flank collapse events exposed in the Guimar, Orotava and Icod valleys, and sea-floor bathymetric studies (Ancochea et al., 1999; Martí et al., 1997; Hunt et al., 2018). The origin of the present Las Cañadas caldera scarp in terms of a pure vertical collapse

hypothesis vs. a giant landslide hypothesis, or a combination of both continues to be debated (for a review, see Martí, 2019).

The Diego Hernandez Formation and the El Abrigo member

The focus of the present work is the Quaternary Diego Hernández formation (DHF), and more precisely its youngest unit, the caldera-forming El Abrigo member. The most recent and detailed stratigraphy of the DHF was provided by Edgar et al. (2007) and considers the DHF to rest directly above the last caldera-forming episode of the Guajara Formation, i.e., the Granadilla member, dated at 600 ± 7 ka by Brown et al. (2003). The DHF is equivalent to Cycle 3 of the Bandas del Sur Formation proposed by Bryan et al. (1998). Thus, the DHF comprises more than 400 ka of explosive eruption activity, in which at least 9 major ignimbrite sheets can be recognized (Brown et al., 2003: Edgar et al., 2007). The total cumulated volume of the DHF is ca. 70 km^3 (Edgar et a., 2007). Coeval basalts, tephrites and mugearites are interstratified with the ignimbrites, especially at the base of the sequence (Neumann et al., 1999; Bryan et al., 2003). Based on geochemistry, three distinct sub-cycles can be identified by different Nb/Zr and Si/Al ratios, a consequence of different fractionation paths (Wolff et al., 2000; Olin, 2007).

The El Abrigo member is the more voluminous ignimbrite of the DHF (> 20 km^3 DRE; Edgar et al., 2007); encompassing almost 30% of the whole volume of the cycle. The widespread distribution of the El Abrigo outcrops, covering almost 360º around the vent, attest to its importance. Several radiometric ages have been published, ranging from 169 to 196 ka (Martí et al., 1994; Brown et al., 2003; Edgar et al., 2007). An inferred

proximal deposit in the Las Cañadas caldera wall has been dated at 179 ± 11 ka (Martí et al., 1994). Its structure and mode of emplacement have been extensively studied by Pittari et al. (2005; 2006), who suggested that the eruption occurred in two distinct pulses separated by a fine ash layer, whereby the ignimbrite body bypassed the upper slopes of the Las Cañadas edifice and deposited in the lower coastal plain, channelized in alluvial valleys or ravines (*barrancos*). In contrast to all the other major ignimbrites of the DHF, Plinian fall deposits appear to be largely absent, although some occurrences were recently identified by Pittari et al. (2006).

The El Abrigo deposits are composed of juvenile clasts dominated by greenish-white, aphyric to weakly porphyritic pumice of phonolitic composition, with subordinate banded and mafic clasts spanning the entire basalt-phonolite range (Nichols, 2001; Pittari, 2004). The proportion of banded and mafic clasts in the deposits is variable, generally ranging from less than 5% up to 40% of the total pumice population, although some well-defined levels in the west coast of the island may reach proportions up to 80% (Pittari, 2004). Phonolitic clasts have a phenocryst assemblage consisting of K-feldspar (*kfs*, sodic sanidine to oligoclase), biotite (*bt*), magnetite (*mag*), ilmenite (*ilm*), and clinopyroxene (*cpx*), with minor apatite (*ap*), titanite (*ttn*), and haüyne (*hau*) (Bryan et al., 2002, Andújar et al., 2008). This mineral assemblage allowed Andújar et al. (2008) to constrain the storage conditions of the phonolitic body before the eruption to pressures of 130 ± 50 MPa (corresponding to 4-6 km depth below the summit), temperatures of 825 ± 25 ºC, water contents of 3 ± 1 wt% and fO_2 at NNO±1. The mafic component is dominated by kaersutite (*krs*), *cpx*, *pl*, *Ti-mag*, *ap*, *hau* and *ilm* (Bryan et al., 2002). Juvenile, glass-bearing syenite is also present, and lithic clasts are abundant and are preferentially

concentrated in a few particular levels (Pittari et al., 2006). A major component among lithics is represented by syenitic clasts, both fresh and hydrothermally altered, originated either at the margins of the El Abrigo magma chamber or in older syenite plutons (Wolff et al., 2000). The coexistence of aphyric and porphyritic pumices, the latter enriched in Ba, Sr, and Eu, suggest that the El Abrigo magma chamber was stratified, with an upper, crystal-poor layer and an underlying lower crystal mush layer which was partially melted and assimilated upon mixing (Nichols, 2001; Sliwinski et al., 2015, Wolff et al., 2020).

Evidence of magma mixing is widespread in the products of the most recent eruptive periods in Tenerife. Although the ignimbrites of the DHF are dominantly phonolitic, a significant mafic portion has been described in at least 5 of them (Aldea, Fasnia, Poris, Caleta, and El Abrigo), which are also accompanied by a variable proportion of mingled pumices (Wolff, 1985; Bryan et al., 2003; Edgar et al., 2007; Olin, 2007). The same is true for many other ignimbrites of the Guajara and Ucanca formations (e.g., Granadilla ignimbrite; Bryan, 2006). This suggests that injection of mafic magmas coming from lower levels of the plumbing system in shallow phonolitic magma chambers had a recurrent and crucial role in the mobilization of the evolved phonolitic bodies and probably triggered the eruptions, with the reheating, melting, and mobilization of crystal mushes playing an important role (Sliwinski et al., 2015; Wolff et al., 2020). However, the evidence of magma mixing in Tenerife is not restricted to the explosive deposits of the DHF. Some historical eruptions of the TPV system produced compositionally zoned lava flows. The most notable of them is the 1100 AD Montaña Reventada eruption, composed of a lower basanite unit and a thick phonolite upper unit, with a fuzzy contact between them (Araña et al., 1994; Wiesmaier et al., 2011).

MATERIALS AND METHODS

Sample collection and preparation

Our sampling locality of the El Abrigo ignimbrite is located in the Bandas del Sur region, at coordinates 28°10'54.61"N, 16°26'42.60"W and 199 m above sea level (**Fig. 1**), at one side of the road from Poris de Abona to Arico, and within the Barranco de Tamadaya. This location belongs to the juvenile-rich Sur-A unit (Pittari, 2004), where banded and mafic pumices represent between 30 and 40% of the pumice population in the deposit. Within the unit, banded pumices are vertically dispersed, without any evident stratigraphic control on their position within the column. Collected samples are representative of the juvenile portion of the Sur-A unit, including white, banded and mafic pumice clasts. In addition, a few indurated lapilli tuff samples representing the finer fraction of the deposit were obtained. From all samples, polished petrographic thin sections (thickness of 30 μm), thick sections (100 μm) and epoxy mounts were produced and used for petrographic observation, geochemical analyses and Raman spectroscopy of glassy groundmass and minerals.

Scanning electron microscopy

A set of high-resolution BSE (Back-Scattered Electrons) images were obtained by Scanning Electron Microscopy (SEM). Two instruments were used: (1) A Field-Emission (FE) scanning electron microscope Zeiss LEO 1525 / Bruker EDX installed at the

Department of Physics and Geology, University of Perugia, Italy, where high-resolution images were obtained with an accelerating voltage of 15 kV and a working distance of 8 mm, for magnifications up to 3000x; and (2) a JEOL JSM IT300LV Scanning Electron Microscope with W source, equipped with an EDS Oxford Instruments X-act Silicon drift detector; operated using the Energy 200 Inca suite software package, located at the Department of Earth Sciences, University of Turin. An accelerating voltage of 15 kV and a working distance of 10 mm were used for magnifications up to 1000x.

Electron microprobe

Concentrations of major elements in glasses and minerals and BSE images of samples were acquired with a Cameca SX100 electron microprobe (EPMA) at the Department of Earth and Environmental Sciences, Ludwig Maximilian University of Munich, Germany. Different settings were used for glass and mineral analysis. For glasses, operating conditions were 15 kV acceleration voltage and 4 nA beam current, and a defocused 5-μm beam was used in order to minimize alkali loss while keeping a good resolution, although where possible, a 10 μm beam was used. For mineral analysis, conditions were 15 kV, 20 nA and focused beam. For both mineral and glass, counting times were 10 s on peak and 5 s on backgrounds at both sides of the peak for all elements. Albite (Na, Al, Si), orthoclase (K), periclase (Mg), apatite (P), wollastonite (Ca), bustamite (Mn), Fe_2O_3 (Fe) and ilmenite (Ti) were used as standards. Standard deviations were lower than 2.5% for all analysed elements. To check precision and accuracy, the basaltic reference glass VG-2 and rhyolitic glass VG-568 (Jarosewich et al., 1980; Helz et al., 2014) as well as

mineral standards NMNH 137041 (anorthite) and NMNH 117733 (diopside) were measured at the start of each analytical session. No significant alkali loss was observed relative to tabulated values of standards.

Laser ablation inductively coupled plasma mass spectroscopy (LA-ICP-MS)

Concentrations trace elements and rare earth elements (Sc, V, Ga, Rb, Sr, Y, Zr, Nb, Ba, La, Ce, Pr, Nd, Sm, Eu, Gd, Tb, Dy, Ho, Er, Tm, Yb, Lu, Hf, Ta, Pb, Th, U) in glasses and minerals (*cpx*, *krs*, *pl* and *kfs*) were obtained by Laser Ablation Inductively Coupled Plasma Mass Spectroscopy (LA-ICP-MS) at the Department of Physics and Geology, University of Perugia. The instrument consists of an Excimer based (λ=193 nm) Teledyne Photon Machine G2 laser ablation device equipped with the two-volume HelEx 2 cell coupled to a Thermo Fischer Scientific iCAP Q quadrupole mass spectrometer (Petrelli et al., 2016a). Circular spots with sizes of 15 and 20 µm were used for glass analyses, and 30 µm for minerals. Ablation times were 30 seconds per spot, preceded by 30 seconds of background measurement and followed by 30 seconds of washout. Laser repetition rate and fluence were set at 10 Hz and 3.5 J/cm^2, respectively. Data reduction was completed with the Iolite software, version 3 (Paton et al., 2011). The analyses were calibrated with the NIST SRM 610 glass (Pearce et al., 1997), and the basaltic glass BCR-2G (Wilson, 1997) was used as quality control. The SiO_2 data obtained by electron microprobe on the same spots were used as internal standard. Analytical precision better than 5% above 20 ppm, in the order of 10% for concentrations in the range 0.1-20, and it

is about 15% for concentrations close to 0.1 ppm. The accuracy is typically better than 10% (Petrelli et al., 2016b).

Raman spectroscopy

Water concentrations were estimated in the glass matrix of the banded and white pumices by micro-Raman spectroscopy. Raman spectra were collected using a LabRam HR800 confocal integrated macro/micro-Raman spectrometer manufactured by HORIBA JOBIN YVON, equipped with a Peltier-cooled CCD detector and edge filters, located at the Interdepartmental Centre "G. Scansetti" (Department of Earth Sciences, University of Turin). A solid-state Nd laser with a wavelength of 532 nm (green light) and power of 80 mW was used as excitation source. A slit of 300 μm and a grating of 600 grooves/mm were used, resulting in a spectral resolution of 1.7 cm^{-1}. Spectra were collected in confocal setting with a hole of 200 μm and the laser was focused on the sample through an Olympus BX41 microscope with an objective producing 100× (spot size resolution of ca. 5×5×15 μm; power at the sample surface of ca. 17.1 mW). Exposure times were of 5x30 s and 10x30 s. The calibration of the instrument was checked at the beginning of each analytical session using the 521 cm^{-1} silicon band. Laser power at the sample surface was checked using a COHERENT "LaserCheck" pen. Spectra were acquired in the 100-1800 cm^{-1} range. Water contents were determined using the methodology proposed by Le Losq et al. (2012), with the previous calibration of the spectrometer response (Shea et al., 2014). For more information, the reader is referred to Supplementary Material 1.

RESULTS

Petrography

Three different petrographic types were recognized: (a) aphyric greenish-white pumice clasts of phonolitic composition **(Fig. 2a)**; (b) porphyritic banded pumices with higher crystal content, ranging from fully developed banded pumices to more irregular and patchy- ones (**Fig. 2b-c**), with variable proportions of mafic material; and (c) aphyric to weakly porphyritic mafic scoriae with numerous greenish-white pumiceous enclaves (**Fig. 2d**). These three sample groups are not sharply separated, but there is a gradation among them. As an example, some scoriae with enclaves seem to gradate to more banded structures within a single large clast (**Fig. 2d**). **Table 1** summarizes the main petrographic features of each group. These different lithologies appear either as bomb-size free clasts to coarse lapilli, or fine lapilli clasts embedded in lithic-rich, indurated lapilli tuffs. Samples from all these lithologies were analysed, as well as two samples of the lapilli tuff.

Lithic-rich lapilli tuff

The sampled outcrop is composed of a lithic-rich lapilli tuff, (samples ABP-F1 and F2, **Table 1 and Fig. 2 b-c**). The samples described here were obtained from the same stratigraphic position as the larger pumice clasts Ii.e. greenish-white and banded

pumices), and thus represents a finer fraction of the sampled deposit, consisting of conglomerates of lapilli-size clasts supported by fine ash. The lapilli-size clasts comprise abundant plutonic lithics (primarily syenites and subordinated gabbros), accidental volcanic rock clasts and juvenile pumice and scoria clasts. The juvenile pumices are mostly phonolitic, but a few banded pumices are present; these pumices are described in their corresponding group (see below). No pure mafic scoriae were identified in these samples, but some glass-bearing, crystal-rich lithic clasts are present. Free crystals (mainly K-feldspar and plagioclase and rare haüyne) are also present, covering the whole grain size range from ash to lapilli. The matrix of the samples consists of glassy ash shards with minor free minerals, some of them attached to glass shards. The glass shards have highly variable shapes, ranging from arcuate, Y- or H-shaped, to fluidal in shape indicating deformation above the glass transition temperature in the eruptive conduit (Giordano et al., 2000; 2005).

White pumices

Phonolitic pumice clasts vary from white to greenish in colour (**Fig. 2a**) and are completely aphyric to weakly porphyritic (extremely scarce phenocrysts of K-feldspar, titanite and magnetite), and highly vesicular (55 to 70% in volume, as measured by image analyses on BSE images). Vesicles are commonly highly elongated reaching cm dimensions and exhibiting a fibrous texture. In some cases, the vesicles are highly anisotropic in shape, exhibiting oriented tubular shapes with equidimensional cross-

sections (tube pumice). Vesicle size and shape vary within a single thin section or epoxy mount scale.

Banded pumices and black scoriae with enclaves

The composite products of the sampled El Abrigo deposits (i.e., those products characterized by different proportions of felsic and mafic material) show a wide range of textures and mineralogical assemblages from banded pumices to black scoriae with abundant detached white-greenish enclaves, and with highly variable proportions of the mafic and felsic components. There is a gradation between these two end-members, and pumices with variable amounts of mafic bands and irregular and chaotic pumices (patchy) are also present (**Fig. 2b-d**). Therefore, the banded pumices and the enclave-bearing dark scoriae are described together below.

Banded pumices vary from strictly banded and laminated (filamentary structure) to more chaotic and patchy clasts. A few highly crystalline mafic enclaves appear entrained in the pumice, with subrounded shapes. Mafic and felsic domains are phenocryst-rich but show different textural characteristics. White domains are analogous to white pumices, i.e., highly vesicular (55% vol), with rounded to elongate and sometimes tubular vesicles, but their crystal content is notably higher. Vesicularity is anisotropically distributed: vesicles are elongated, usually parallel to the contact with the dark domains. Phenocrysts represent 20% in volume and are composed of *kfs*, *bt*, *mag* and *ap*. Alkali feldspar phenocrysts are usually aligned following the banding and vesicle anisotropy. Mafic bands in the banded pumices are filaments, with widths ranging from 1-2 cm to less than

1 mm and representing a widely variable proportion of the clast (**Fig. 2**). In hand samples, they are frequently folded and contain sparse mm-size phenocrysts (*krs*, *cpx*, *pl*, *kfs*). Phenocrysts represent ca. 20-30% and are set within a highly vesicular matrix (52% vol. porosity). Vesicles are small, equidimensional, and well connected, and no clear anisotropy is present. Coarser filaments are usually finely crystallized, with a high proportion of microlites, but the thinner filaments are frequently fully glassy (**Fig. 3**).

The black scoriae are finely vesiculated, although vesicularity is high (62-70 vol. %). The phenocryst content is lower than that of the banded pumice (ca. 20 vol. %) and consists of *kfs*, *cpx*, *krs*, *pl*, and Fe-Ti oxides, with lesser *bt* and *ap*. The phonolitic enclaves within the collected scoria samples represent ca 10 - 15 vol. % of the rock and have very elongated, sometimes folded shapes. Enclaves are almost aphyric, showing only scarce *kfs* phenocrysts. They show a low vesicularity compared to white pumices (35-40 %). Their contact with the mafic host is sharp in the hand-sample scale but becomes very complex, chaotic-looking when observed at the microscope, developing convoluted small-scale interaction structures (**Fig. 3**).

Noteworthy are the small-scale interaction textures present in all mixed pumices between mafic and phonolitic melts. In white enclaves from dark scoriae (samples ABP-M), complex filaments and bands of mafic melt extend inside the phonolitic enclaves, showing shapes ranging from very thin filaments to coarser bands (widths from <10 μm up to 500 μm; **Fig. 3**). Also, the contact between the enclaves and the mafic host often exhibits a very complex structure, with festoons and flames of mafic melt protruding into the phonolite (**Fig. 3d**). While the phonolite melt is completely aphyric, the mafic melt has variable degrees of crystallization, with the coarser bands showing the highest

proportions of crystals. Their mineralogy consists mainly of clinopyroxene, Fe-Ti oxides and plagioclase, with minor apatite. On the contrary, thin, hybridized filaments carry very few or no crystals at all.

In the banded pumices, complex interaction structures are much harder to find, and where visible, they are less complex (**Fig. 4**), with some festoons or filaments. Contacts between the phonolite and the mafic melt are usually well defined, and the mafic melt is more pervasively and finely crystallized than in the mafic scoriae. The comparison between structures in the mafic scoriae and the banded pumices seems to indicate that the former represents a more evolved state in the mixing process, with a more quenched melt and higher viscosity contrast.

Mineral content of the banded pumices and scoriae

Since the phonolitic pumices are almost completely aphyric, this section will only describe the mineral assemblage of the composite products. Both products have an almost identical crystal content, although with different proportions and chemistry of minerals. Two different assemblages can be distinguished, belonging to mafic domains and the felsic domains in the banded clasts, respectively. Assemblage I is found in the mafic domains and is characterized by *cpx + krs + pl + kfs + mag*, with lesser amounts of *ap + bt + ilm*, and assemblage II is found in the felsic domains, consisting of *kfs + bt + mag + ap*. In the crystal-rich banded pumice, the full population can be found, whilst KFs is the main component of the felsic enclaves in the mafic scoria. **Table 1** reports a summary of the mineral content of each group.

Plagioclase

Plagioclase phenocrysts are found only in the mafic domains of the composite products (assemblage I). Phenocrysts are subhedral, and range in length from 0.3 to 1.7 mm and width of 0.1 to 1 mm, with a typical aspect ratio of 2:1 to 4:1. Cores frequently show sieve texture. Compositionally, *pl* range from bytownite to andesine ($An_{83}Ab_{16}Or_1$ to $An_{41}Ab_{56}Or_3$), with compositions comparable to plagioclases in the DHF tephrites ("Cycle 3") from Bryan et al. (2002) (**Fig. 5a**). No consistent zonation was detected in BSE images or by comparing rim and core compositions, although a subgroup displays a sieved core. Microlites are euhedral and acicular to tabular, 30 to 100 μm in size, and show frequent zoning in BSE images. There is no apparent compositional distinction between phenocrysts and microlites, although the latter tend to be more calcic and have a more restricted composition. Among the trace elements, phenocrysts show variable contents of Ba (300-3200 ppm), Sr (2200-4600 ppm) and Eu (1,4-2,7 ppm), are found, although only 5 LA-ICP-MS analyses in 5 different crystals are available (see Supplementary Materials). Melt embayments and inclusions are common in phenocrysts, and the latter appear preferentially in the sieve-texture cores of the most calcic plagioclases (An_{55-83}). Glasses in these inclusions represent the most primitive glasses found in the studied samples.

Alkali feldspar

Alkali feldspar phenocrysts are common in composite pumices in both felsic and mafic domains (assemblages I and II). They occur as tabular crystals, often with prominent Carlsbad twinning and with lengths ranging from 0.3 to 4.5 mm, widths of 0.1 to 1 mm, and aspect ratios of 1:5 to 1:10. Crystals in the felsic bands are euhedral to subhedral and frequently fractured, while those in the mafic domains show more evident signs of disequilibrium, in the form of common resorbed rims and subhedral to anhedral shapes. Compositionally, they are orthoclase to sodic sanidine ($An_{10}Ab_{73}Or_{17}$ to $An_{2}Ab_{60}Or_{38}$), with no obvious zoning observed (**Fig. 5a**). However, trace elements are widely variable between individual crystals, such as Ba (38-9740 ppm), Sr (16-846 ppm), Rb (8-73 ppm) or Eu (0.5-3.9 ppm), and all of them except Rb show well defined negative correlations with X_{Or} (Figure S3 in Supplementary Material 1). Minerals in the crystal-rich banded pumice are Ba, Sr, and Eu-rich, contrasting to those found in the mafic scoria, with notably lower concentrations. However, the reverse is true for Rb. These textural characteristics indicate that K-feldspars are original from the phonolitic component, probably representing a disrupted crystal mush (e.g., Silwinski et al., 2015; Wolff et al., 2020), and that ubiquitous crystal transfer and entrainment to the mafic melt has occurred.

We note that a subgroup of K-Feldspar phenocrysts shows prominent microperthitic exsolutions. These crystals are texturally distinct from the former group, showing highly anhedral and equidimensional shapes. The albitic end-member in perthitic crystals is well defined, being albite orthoclase with up to Or_{20}; and K-Feldspar end-member is Sanidine with up to Or_{91}. Given the average compositions and proportions of end members, these data suggest that perthites originate from unmixing of an Orthoclase feldspar. Perthites

are present in syenitic lithics in El Abrigo deposits which indicate cooling to temperatures below 560°C before the eruption (Wolff et al., 2000). Hence, the perthitic feldspars in the banded pumices can be classified as xenocrysts.

Clinopyroxene

Cpx belongs only to assemblage I and appears exclusively in the mafic domains, as two different populations: phenocrysts and microlites. Scarce phenocrysts range from 0.2 to 1.8 mm in size and are frequently associated with apatite (forming rounded inclusions hosted by the pyroxenes) and *Ti-mag*. Crystals are subhedral to anhedral, displaying rounded corners and resorbed rims, indicating that they are in disequilibrium with the tephriphonolitic groundmass glass. Compositionally, they are a very homogeneous group, classifying as diopsides with a very restricted composition ($En_{39-41}Wo_{46-48}Fs_{12-15}$) with Mg# ranging from 69 to 78 ($Mg\# = 100 \cdot MgO/(MgO+FeO_t)$ on a molar basis, with FeO_t being total Fe expressed as FeO).

The second pyroxene population appears as small microlites in the mafic domains, including the thin, hybrid bands dispersing in the phonolitic enclaves. They represent the most abundant phase in the groundmass mafic glass and appear as prismatic crystals in sizes ca. 10-50 microns. They often show signs of rapid growth, such as pointed apices or dendritic textures (**Fig. 4f**). EPMA measures show that these pyroxene microlites differ in composition from the phenocrysts ($En_{30-35}Wo_{46-51}Fs_{17-20}$, Mg# 60-68), being notably silica-poor and Al and Ti-rich (**Fig. 5b**), and are frequently zoned, with a brighter rim in BSE images (**Fig. 4f**). A third population of pyroxenes is defined by dendritic and

acicular crystals, sometimes pervasively crystallizing in the mafic melt and frequently coating the surface of plagioclase microlites.

Kaersutite

Kaersutitic amphibole phenocrysts are more abundant than *cpx* and are only present in assemblage I as euhedral to subhedral crystals, sometimes with rounded corners, ranging in size from 0.5 to 1 mm, equidimensional (basal sections) to very elongated, and frequently fractured. Basal sections show well developed cleavage. Inclusions of *ap* and Fe-Ti-oxides are common. In the EPMA, 24 analyses were obtained in 9 different grains, from which formula units were calculated using the mass-based model of Ridolfi et al. (2018). Results show that all amphiboles are classified as kaersutites with a very homogeneous composition (#Mg 66-69) and are Si-poor (5.8-6.1 atoms per formula unit, apfu). Estimated structural H_2O ranges between 0.8 and 1.2 wt%. No consistent variations are found between crystal cores and rim regions.

Biotite

Biotite is a common phenocryst, belonging to both assemblages I and II as euhedral crystals with sizes 0.4 to 1.4 mm, frequently associated with apatite and oxides. Apatite appears as well frequently as inclusions in biotite. Compositionally they straddle the transition between phlogopite and biotite and are Mg rich (Mg# 60-70). All aluminium occurs in the tetrahedral site. Assemblage II biotites (felsic domains) are classified only

as phlogopites and their composition is more restricted than in assemblage II (mafic domains), having higher Mg# (0.67-0.68), Ti, and lower Fe. However, there is an overlap in composition in both populations. This agrees with Bryan et al. (2003), who described two distinct populations based on Ti content and an inverse relationship between Fe and Ti in El Abrigo pumices. Wider dispersion in composition in the mafic domains could be a consequence of the more heterogeneous composition of the mafic melts since biotite appears to be extremely sensitive to liquid composition (e.g., Sliwinski et al., 2017).

Fe-Ti Oxides

Fe-Ti oxide crystals appear in both assemblages from mafic and felsic domains but are much more abundant in the former. They occur both as isolated phenocrysts and in association to or forming inclusions in clinopyroxene, kaersutite, and apatite; always with rounded to subrounded shapes. They are classified mainly as titanomagnetite, but a few ilmenites are also present in the dark bands. The composition of magnetite is bimodal, with two distinct groups evident in classification diagrams. One group is Mg-poor, richer in Fe^{2+} and Mn and lower in Ti+Cr and includes the only analysis from white pumice as well as the few crystals from enclaves. This group overlaps with natural and experimental magnetite from the El Abrigo phonolite (Andújar et al., 2008) and the phonolitic magnetites from Bryan et al. (2002) (**Fig. 5d**). The more abundant second group, frequently associated with *cpx* and *krs*, is Mg-rich (6-7 wt%), Fe^{2+} and Mn-poorer, and slightly higher in Ti+Cr. This group overlaps partially with magnetite from the Cycle 3

basalts and tephrites from Bryan et al. (2002). The molar fraction of Ulvöspinel endmember (Usp) in titanomagnetite ranges from 0.34 to 0.51.

Apatite

Apatite appears as euhedral to subhedral crystals, ranging in size from phenocrysts (0.1-0.5 mm) to microlites (< 50 μm). Phenocrysts are associated with clinopyroxene, Fe-Ti oxides, and biotite, or forming rounded inclusions in them. Some apatite phenocrysts also show rounded inclusions of phonolitic melt.

Glass chemistry

In total, approximately 320 points of glass matrix were measured by the electron microprobe in three types of products (5 white pumice clasts, 3 banded pumice clasts, and 1 mafic scoria with enclaves, in addition to free glass shards in the lapilli tuff sample). In addition, 172 of these points were reanalysed for trace elements by LA-ICP-MS, taking special care on measuring the same spot. The locations of the analytical spots were carefully selected to avoid the presence of crystals, but in some places of the banded pumice sample, this was impossible to achieve due to the high degree of crystallization and the small size of the crystals. In such places, the analytical data approximates the bulk composition of the melt before crystallization (glass + crystals). Analyses with closure >94% were considered valid, due to the high H_2O content in the glasses (more details about H_2O content estimates are provided below). Major element analysis recalculated on a volatile-free basis show a wide range of compositions, spanning the

complete compositional range from phonotephrite (ca. 51-52 wt% SiO_2, 3 wt% MgO, and 9 wt% alkalis) to phonolite (ca. 61 wt% SiO_2, 0.3 wt% MgO ad up to 16 % alkalis).

Some particularities can be readily observed in the different sample groups. White to greenish pumices (including glass shards) are phonolitic and show a conspicuous shift in composition marked by a clear Na enrichment from the trachyte-phonolite divide in the total alkali-silica diagram (**Fig. 6**). Total alkalis increase from ca. 12-13 wt% to 16 wt%, and in this trend, Na_2O increases from ca. 7.5 wt% to 10 wt%, while SiO_2 contents decrease from 63 wt% to 59 wt% (**Fig. 7**). The trend is common in several of the phonolitic units in the DHF (Bryan et al., 2002; Sliwinski et al., 2015), and results from the fractionation of phonolites and trachytes towards the phonolite minimum, away from the alkali feldspar thermal divide (Schmidt and Weidendorfer, 2018). However, trace elements discriminate two phonolitic glass groups: (a) high-Zr (HZ) and (b) low-Zr (LZ) phonolite (**Fig. 8**). The HZ group shows Zr concentrations between 860 and 1400 ppm, low Ba (<100 ppm) and Sr; and high Nb, U, and Th. High Na_2O (14-16 wt%) and Al_2O_3 (up to 20 wt%) are also characteristics of this group. On the other hand, in LZ glasses, Zr concentrations range from 400 to 800 ppm and are accompanied by high Ba (up to 800 ppm) and low alkalis (13-14 wt%). In the OIB-normalized spider diagrams (**Fig. 9**), this translates into deep Ba and Sr negative anomalies and Zr positive anomalies in the HZ glasses, which are also characterized by enrichments in Th, U and Nb relative to Zr-poor glasses. LZ glasses are represented not only in the white pumices but also in the banded pumice sample. In addition, the HZ group is not well separated from the LZ group but seems to be mixed in a heterogeneous reservoir (i.e., in a single pumice class both types may be present).

In the composite products, variation in glass chemistry is notably higher, covering the whole range between phonotephrite to phonolite, with some data points straddling the divide to benmoreite and trachyte **(Fig. 6**); and compositions are well correlated to the distinct mafic and felsic domains observed in them. This differs from some other banded pumices described in the literature (e.g., Krakatau; Self, 1992, or Vulcano; Rossi et al., 2019) in which interstitial glasses in banded pumices do not show a large variation in chemistry but do in crystallinity and vesicularity. In the El Abrigo banded pumices, the upper compositional range (corresponding to white bands in the banded pumice) overlaps with the Na-poor phonolitic glasses of the white pumices. A mixed lapilli clast in a tuff sample (**Fig. 4e**) shows an identical trend. In contrast, glass composition in the mafic scoriae overlaps the whole range of compositions of the white pumices. The least evolved compositions are always found in the dark domains and filaments (**Fig. 3**), although these domains show a wide compositional range, varying from phonotephritic to phonolitic even at short distances. In addition to this, it also stands out that glasses in the enclave-rich mafic scoria and the mixed lapilli clast show a slightly wider compositional range than in the banded pumices (**Figs. 6 and 7**). The most mafic glasses in the enclave-rich scoriae are ca. 2-3 wt% more depleted in SiO_2, ca. 2 wt% enriched in FeO_T and 1-1.5 wt% enriched in MgO relative to the least evolved glasses in the banded products. V concentrations also have a wider range in those products compared to the banded pumice, with V concentrations reaching up to 220 ppm (**Fig. 8**). Overall, glass compositional ranges found in this work are larger than those found by Wolff (1985) for the Tajao ignimbrite, and by Wolff et al. (2020) in the El Abrigo and Porís ignimbrites and expand the available dataset for the El Abrigo eruption.

In the binary variation diagrams **(Fig. 7**), linear trends are found in most major oxides, while non-linear trends appear in Al_2O_3 and Na_2O. Particularly, Na_2O shows a mild bell-shape that has been previously observed in mixed volcanic products (e.g., Turnbull et al., 2010; Morgavi et al., 2016; Laeger et al., 2019; DeVitre et al., 2019), and is indicative of diffusive fractionation of the fast-diffusing Na relative to the remaining, slower components. This arcuate shape is visible when comparing Na_2O to CaO or TiO_2, i.e., elements with contrasting diffusivity. Nonlinearity in binary diagrams is clear evidence of diffusive equilibration playing a key role in the chemical evolution of the system (see Discussion).

Among the trace elements, several divergent behaviours are observed in the different mixed products. Concentrations of Ba and Eu are notably higher in the most mafic and intermediate glasses in the banded pumice (reaching up to 1740 ppm Ba), while in the mafic scoria Ba levels do not exceed ca. 1000 ppm and are fairly constant. These trends mimic those reported by Wolff et al. (2020) (glass) and Sliwinski et al. (2015) (whole rock). The OIB-normalized trace element spectra (**Fig. 9b-d**) illustrate well these differences. Strong Ba and Sr negative anomalies are present in phonolitic glasses, while positive Ba anomalies are found only in mafic and intermediate glasses of the banded pumice. Similarly, the positive Zr anomaly and enrichments in Th, U, and Nb visible in the HZ phonolitic group is also present in the phonolitic enclaves of the mafic scoria but absent in the other two composite clasts.

Several melt inclusions located in the sieve-textured cores of plagioclase phenocrysts and some melt embayments were measured in the two banded pumice samples (15 analyses in 5 different crystals). Their high P_2O_5 and K_2O levels, and low Al and Ca

suggest that their composition was modified by post-entrapment crystallization (PEC; Kress & Ghiorso, 2004). To retrieve their original composition, a PEC correction was performed by adding amounts of 10 to 25% of host plagioclase to the inclusion, to make them fit with the general trends of the Tenerife geochemistry (following the procedure of Neave et al., 2017). After PEC correction, these glasses are the most mafic ones measured in our sample set, and span from basanite to tephriphonolite (SiO_2 45.1-54.6 wt%, MgO 5.6-1.6 wt% and alkalis 5.5-11.4 wt%) and probably represent relics of the more primitive magma parental to the mafic end-member. Two melt embayments in one plagioclase crystal revealed a phonotephritic composition, slightly more mafic than the most primitive groundmass glasses.

Raman spectroscopy shows that all El Abrigo glass matrixes are water-rich, which is also in agreement with relatively low totals in EPMA analysis (94-98 wt%). Analysis following the method of Le Losq et al (2012) (see **appendix**) suggests that overall, residual H_2O contents range from 0.5 to 5.7 wt%. The distribution of H_2O concentration through all sample groups is bimodal (**Fig. 10**), with modes of 0.8 and 3.3 wt%, however, white pumices are on average more hydrous (average of 3.3 wt%) than mixed products (1.3 to 1.9 wt% in banded and mafic pumices, respectively). The discrimination of glass type independently of sample type offers a similar dichotomy, with phonolitic glasses averaging 2.8 wt%, versus 1.9 wt% for mafic glasses.

DISCUSSION

Chemical heterogeneities in the plumbing system

One of the most important pieces of information when studying magma mixing processes in volcanic systems is the precise characterization of the end-members involved in the process. In cases where the mixing event has had enough time to progress efficiently, one or both involved magmas is usually lost, by progressive blending into a hybrid composition. Due to its faster diffusion kinetics and its lower relative proportion, the more mafic end-member is the first to be lost. However, an efficient mixing between magmas of high compositional and viscosity contrasts is usually difficult to achieve in nature, leaving behind mingling textures in quench products. In El Abrigo, the abrupt termination of the mixing process by the eruption and the proportions of the mixing magmas favoured the conservation of the more evolved melt in the deposit, represented by LZ and HZ phonolitic pumices.

However, the mafic end-member poses some more difficulty. The least evolved glasses in the mixed products (especially the enclave-rich scoriae) have a phono-tephritic composition, of ca. 51 wt% SiO_2, 3 wt% MgO, and 9 wt% alkalis, but their low frequency among analysed spots suggests that the original mafic melt is close to being lost, due to its lower proportion relative to the phonolitic endmember and faster diffusion kinetics. Whole-rock analyses of mafic pumices and scoriae (Nichols, 2001; Pittari, 2004) indicated that a possible end-member could be a basanite or, more probably, a tephrite with a composition similar to the DHF Cycle 3 tephrite of Bryan et al. (2002). The examination of the crystal content of the mafic domains of the mixed products, with the presence of kaersutite and plagioclase phenocrysts but lacking olivine, supports the case for a tephritic to phonotephritic end-member rather than basanitic in terms of whole-rock

chemistry. The mineral assemblage of late-stage DHF phonotephrites is composed of *krs+cpx+mag+ap* (Bryan et al., 2002) and is consistent with the mineral assemblage and mineral chemistry observed in the mafic domains of the El Abrigo composite products. Moreover, geochemical modelling suggests that tephrites and phonotephrites are a common step in the fractionation series of Tenerife from a parental basanite (Sliwinski et al., 2015). The distribution of the mineral phases between mafic and felsic domains indicates that crystal transfer proceeded prevalently from the phonolite units towards the mafic units. As an example, *kfs* are widely present in mafic domains, but *krs*, *cpx*, and *pl* rarely occur in the phonolitic domains.

In this context, the plagioclase-hosted melt inclusions potentially provide a complementary point of view, representing a relic of the primitive magma precursory to the tephrite. In basanitic melts, and especially in hydrous ones, plagioclase is not a liquidus phase and only crystallizes at lower temperatures (e.g., Iacovino et al., 2016). As indicated by the sieve-textured cores in which the more primitive inclusions are found, host plagioclase is not in equilibrium with this basanite, indicating that the melt inclusions were trapped in refilling events of the tephritic magma reservoir at the base of the crust. In the basis of this evidence of melt-plagioclase disequilibrium and broad similarity to Tenerife basanites, we suggest that the lower crustal tephritic reservoir was periodically replenished by basanitic magma before the ascent and encounter with the shallow phonolitic reservoir, thus pointing to the occurrence of an earlier mixing event in the El Abrigo plumbing system.

H_2O contents in the El Abrigo glasses

The distribution of H_2O contents in the glass matrix of banded pumices and dark scoriae raises the question of the origin of these high- H_2O contents. Although the upper mode (3.3 wt%) of these values seems to agree with amphibole and alkali feldspar hygrometry obtained in this work (see following section), these values are also remarkably similar to equilibrium H_2O contents attained from meteoric absorption of H_2O in glasses (ca. 3-4 % H_2O; Seligman et al., 2016). The variability of H_2O contents measured in our glasses, which does not correlate well to glass composition, seems to indicate that current H_2O in glasses is mostly of meteoric origin and not residual magmatic H_2O. This is also in agreement with the incipient depletion in Na and K observed in a few of the glass analyses, which are due to slight meteoric alteration, even though they do not show any other sign of it. However, it should be noted that Piochi et al. (2008) found medium-high H_2O contents (2-3 wt%) in Campi Flegrei pumices that are interpreted as residual dissolved H_2O based on correlation to Cl contents. Hence, further work is necessary to clarify the origins of present H_2O contents in the El Abrigo pumices.

Mineral-melt thermobarometry and hygrometry

To shed light on the origin and storage conditions of the end-members, we explored possible mineral-melt equilibria using available igneous thermometers, barometers, and hygrometers. For each mineral group, minerals do not fulfil equilibrium tests with the coexisting, hybrid melts, hence different possible equilibrating melts were tested for each mineral group. These were: (a) high-Zr phonolite (HZ), taken as the average composition

of pumice clast ABP-F/PC3; and (b) the average of the five most mafic interstitial glasses found in the mafic pumices, of phonotephritic composition (hereafter referred as PT51). A summary of thermobarometric calculations is given in **Table 2** and **Fig. 11**, and the complete composition of the chosen equilibrium melts is given in the Supplementary Materials.

The amphibole thermometry proposed by Ridolfi and Renzulli, (2012) and revised by Ridolfi (2021) was used to explore possible equilibria of kaersutites in the banded pumices. Results suggest amphibole crystallization took place at 451 ± 43 MPa and 1056 ± 12 ºC. The predicted H_2O amount in this melt is 2.9 ± 0.5 wt%, although *krs* compositions are slightly outside the calibration range for water contents. The calculation of the potential equilibrium melt suggests that kaersutites crystallized in a Si-poor melt (49-53 wt% SiO_2), although this equation is calibrated in calk-alkaline melts and these values must be taken as indicative only. Although some care needs to be taken with amphibole barometric results (e.g., Erdmann et al., 2014, Putirka, 2016), the degree of agreement with *cpx* barometry allows to reinforce their validity. Moreover, both *cpx*-melt and *krs* thermo-barometry suggest a silica-poor melt phase similar to the most mafic analysed glasses was present immediately before mixing.

Clinopyroxene-melt equilibria were explored using the thermobarometric calibration of Masotta et al. (2012), which is calibrated for alkaline melts (tephriphonolites and phonolites). *cpx* phenocryst rims fulfil equilibrium tests (Rhodes diagram, **Fig. 11**) when paired to the PT51 glass composition, of ca. 51.1 wt% SiO_2 and 3.3 wt% MgO (Mg# 46). Following amphibole thermobarometry, a water content of 3 wt% was assumed for the calculations. Estimates result in an average temperature of 1044 ± 8 ºC and pressure of

412 ± 38 MPa for 23 mineral-melt pairs. An attempt was made to explore the equilibria of *cpx* microlites with their coexisting hybrid melt (Mg# 32-35). Although such pairs pass the equilibrium test, their thermo-barometric results show a very high uncertainty probably arising from incipient equilibrium and rapid growth, and hence they were discarded as reliable thermobarometers.

Among plagioclases, only labradoritic and bytownitic plagioclase rims pass the equilibrium test proposed by Putirka (2008) when paired with the PT51 glass composition. With such parameters and assuming the pressure and H_2O contents obtained from Amphibole and *cpx*-melt equilibria (average of 431 ± 57 MPa and 3 wt% H_2O), temperature estimates result in an average of 1044 ± 7 ºC (22 mineral-melt pairs). However, given the hydrous nature of the El Abrigo system, this value should be taken only as an upper limit, since in hydrous systems plagioclase saturation always occurs below that of *cpx*. Likewise, the hygrometric calculation of Waters & Lange (2015) results in H_2O contents of 1.8-2.1 w% for the melt phase, but this result should be regarded only as a minimum value.

On the other hand, alkali feldspars appear to be in equilibrium with a phonolitic melt similar to the most evolved, high Zr phonolite represented by the white pumices, using the equilibrium test proposed by Mollo et al. (2015). Mineral-melt pairs not exceeding a 10 % difference between measured values of $K_D^{Or\text{-}Ab}$ and those predicted by Mollo et al. (2015) were used. The employment of the Putirka (2008) thermometer, using the pressure obtained by Andújar et al. (2008) as input (130 ± 50 MPa), gives temperatures of 893 ± 9 ºC as a result. Using the same data as input in the Mollo et al (2015) hygrometer produces a result of 4.1 ± 1.1 wt%% for the phonolite, very similar to estimations by Andujar et al.

(2008); although it should be noted that the Mollo et al. (2015) model is calibrated with their data. Direct measurements of water contents by Raman spectroscopy (this work) also agree well with this result, although its significance as magmatic water is unlikely.

Taken together, the explored mineral-melt equilibria draw a remarkably consistent picture for the pre-mixing mafic end-member and can also be used to extract some insights on the storage conditions of the phonolite body. As obtained from *krs*, *cpx*, and *pl* phenocrysts, the mafic endmember was stored at ca. 1050ºC and 412-450 MPa, with water contents of 3 wt%. The corresponding equilibrium melt under these conditions was phonotephritic in composition, with ca. 51 wt% SiO_2 and 3-4 wt% MgO. The obtained pressure values suggest that the tephritic magma was stored at a depth between 12 and 15 km. These depths are in good agreement with geophysical estimates of Moho depths in Tenerife (ca. 15 km, Lodge et al., 2012; Martinez-Arevalo et al., 2013). Storage at Moho depths seems to be common in other Atlantic Ocean islands, as evidenced by thermobarometry and geophysics (e.g., Beier et al., 2006; González et al., 2013; Oglialoro et al., 2017). Our pressure estimates fill a gap between a mantle storage region of basanites (ca. 700 MPa, Neumann et al., 1999) and the shallow phonolitic chambers (ca. 150 MPa, Andújar et al., 2008). Furthermore, our temperature estimates are identical to magnetite-ilmenite thermometry in the mafic portion of banded pumices from other ignimbrite bodies in the DHF (1050°C, Bryan et al., 2002), suggesting a protracted storage region for tephritic-phonotephritic magmas in Tenerife during DHF activity. In turn, the phonolitic end-member could have equilibrated at ca. 890ºC (assuming a pressure of 130 MPa, Andújar et al, 2008). This temperature is higher than that of

Andújar et al. (2008), although it could reflect conditions in the upper, crystal-poor and Zr-rich phonolitic reservoir, as opposed to a crystal rich, mushy reservoir.

Role of mush/cumulate melting and magma mixing

The various pieces of information presented in this work support that the mixing event that preceded the El Abrigo eruption was complex and included the disruption and melting of a pre-existing cumulate and/or crystal mush by the incoming magma, which immediately preceded and superimposed upon the incipient chemical hybridization of the melt phase. Moreover, different collected samples seem to suggest a different combination of processes.

The presence of partially resorbed sanidine and anorthoclase crystals in the mafic domains of two of the composite clasts, coupled to the prevalence of high Ba, Sr, Eu, and low Zr (**Fig. 8**) in their mafic to intermediate glasses, is clear evidence of the interaction between the mafic magma and a K-feldspar rich phonolitic reservoir. These observations are in line with those of other authors (e.g., Edgar et al., 2002; Wolff et al., 2015; Sliwinski et al., 2015; Wolff et al., 2020), for El Abrigo and other zoned ignimbrites in Tenerife and elsewhere. In this view, the low-Zr phonolitic glass is the product of partial melting of the alkali-feldspar-rich mush, enriched in Ba, Sr and Eu (elements that partition strongly into feldspar) but depleted in Zr, Th, or Nb. Rb contents in these glasses are low, but are in consonance with Rb contents measured in K-feldspars in the same samples (Supplementary Material and **Figs. S3 and S4**). On the other hand, the crystal-poor, high-Zr phonolitic melts found in the white pumices represent an evolved melt

extracted from the mush zone during the development of the magma chamber, from which alkali feldspar and biotite have been removed (Sliwinski et al., 2015).

However, the degree of assimilation of the mush/cumulate seems to vary between samples, and the analysis of the mafic scoria show only minor to no enrichment in Ba, Sr, and Eu in the intermediate glass, accompanied by large variability in Zr contents. The degree of crystallinity of these clasts is lower than the banded pumice, especially in its phonolitic domains which are almost completely crystal-free. We suggest that the mafic scoria represents the interaction of the mafic end-member with a different, crystal-poor, and chemically heterogeneous phonolitic zone inside the El Abrigo magma chamber, constituted primarily by an evolved melt extracted from the crystallizing mush in lower zones of the reservoir. Heterogeneities within this reservoir could be related to the dissolution of small quantities of alkali feldspar upon heating before mixing with the mafic magma, or by mixing between high-Zr and low-Zr phonolites immediately before contact with the tephritic magma (as suggested for the Fasnia member of the DHF by Olin, 2007), which may have been triggered by buoyant overturn of the silicic reservoir upon mafic injection (e.g., Bain et al., 2013). Previously published data for the Poris member of the DHF (Wolff et al., 2020; Edgar et al., 2002) suggest that in that unit the mafic magma interacted only with the Low-Zr phonolite. However, our study suggests that at least in the El Abrigo system, it interacted also with the high-Zr phonolite, although perhaps in a more limited way.

The second process influencing the chemical variability in El Abrigo is magma mixing itself. Upon the interaction of two compositionally distinct melt phases, a diffusive mass exchange starts between them. Diffusion is a slow process, and it cannot alone leave its

signature in large volumes of melt, but it is in turn notably enhanced by physical mingling (De Campos et al., 2008). Chaotic mixing dynamics frequently develop during mixing processes, where extensive stretching and folding of the involved magmas result in complicated structures from micro to macro scales (e.g., Perugini et al., 2003; Morgavi et al., 2013; 2016). These structures provide large melt-melt interface areas through which the diffusive process progresses, significantly enhancing its efficiency. Although classically mixing events were thought to result in linear interelement patterns, recent research (Perugini et al., 2008; Morgavi et al., 2013; Perugini et al., 2015; González-García et al., 2018) has shown that this is not necessarily the case due to the different diffusivities observed among chemical elements. This triggers a diffusive fractionation process, which can be recognized in mixed volcanic rocks, especially those where the mixing process is far from being complete. Also, melt-melt partitioning can be superimposed to diffusion in some elements depending on the arrangement of the end-members in the compositional space (Chakraborty et al., 1995; González-García et al., 2018), further complicating the chemical evolution of the system.

Evidence of mixing in the El Abrigo pumices is found examining some major and trace element distributions in the glass phase. Pairs of elements with similar diffusive behaviour result in mostly linear trends (e.g., SiO_2, TiO_2, CaO, MgO; **Fig. 7**). On the contrary, the arcuate shape of the Na_2O vs SiO_2 variation diagram between the two inferred end-member compositions of the mixing process (tephrite and phonolite), also reflected in the TAS diagram (**Fig. 6**), can only be explained by significantly larger diffusivity of Na compared to the remaining major elements. Experimental data suggest that Na diffusion in alkaline intermediate to silicic melts is notably faster than that of Si,

Ti, or Mg (Zhang, 2010; Perugini et al., 2015), and contrary to most other elements, shows faster diffusion in silicic melts (Zhang et al., 2010). Arcuate Na_2O trends have been observed before in composite volcanic products (e.g., Morgavi et al., 2016; DeVitre et al., 2019), and have been reproduced in both static and dynamic mixing experiments (Morgavi et al., 2013; González-García et al., 2017; Rossi et al., 2019).

The idea of diffusive fractionation can be better visualized by statistical treatment and elemental imaging. **Fig. 12** shows a set of elemental maps obtained with the SEM, coupled to histograms illustrating the different chemical distributions of Si, Mg, and Na in glasses. Whilst Si and Mg are good tracers of the different compositional domains and exhibit steep gradients, in the Na image such structures are hard to identify due to a much more homogeneous concentration. Likewise, compositional histograms of Si and Mg in all composite pumices are bimodal to notably skewed, whereas the Na histogram is almost unimodal.

From this information, some qualitative constraints can be put in the time scales of the mixing process. The wider compositional range observed in the mafic scoria and the mixed lapilli in comparison to the banded pumice suggests that the former two represent two different stages of the mixing event, assuming that the input mafic melt was compositionally homogeneous during the whole event. Furthermore, the complexity of the mixing structures is also higher in the former two clasts than in the banded pumice. **Fig. 13** shows a selection of EPMA transects across filamentary structures near the contact between phonolitic enclaves and the host mafic scoria. In all three transects, it is evident that the thin filaments are more hybridized than the thick ones, which also prevented their crystallization upon cooling because of the slower diffusion kinetics.

Also, the contact between phonolitic and mafic melt is gradual, especially in the MgO and Na_2O profiles. The preservation of these small-scale structures (less than 100 µm thick) is indicative of very short mixing timescales, possibly in the order of few hours (Laeger et al., 2017; Rossi et al., 2019). On the contrary, the lower degree of complexity in the banded pumice is indicative of somewhat longer mixing timescales. In this case it is not possible to extract mixing timescales from direct diffusion modelling, mainly due to the complexity of mixing dynamics in the system (i.e., the lack of knowledge of the convection field). Similar small-scale filament-like structures and interdigitations have been described on the island of Ascension (Chamberlain et al., 2020) and Turrialba volcano (DeVitre et al., 2019), where the authors also inferred short magma interaction timescales.

The interplay between crystal melting and magma mixing can be summarized in a ternary trace element plot (**Fig. 14**). Elements Ba, Zr, and V have been chosen as tracers of both processes, where the Ba axis is a proxy for feldspar melting and the V-Zr axis is indicative of mixing between end-member magmas. Three different compositions, already discussed in preceding sections, are proposed as end-members for the mixing event. The mafic end-member plotted is a tephrite with the composition of the Cycle 3 tephrite in Bryan et al. (2002), with 730 ppm Ba, 464 ppm Zr and 188 ppm V. This tephrite is related to parental basanites by fractional crystallization processes but mixing between basanite and tephrite is likely involved, as reported in previous sections. The melt component of this tephrite prior to the mixing event is inferred to be phonotephritic with a composition akin to the PT51 glass used in pyroxene-melt equilibrium calculations. In the other end of the compositional spectrum, two phonolitic compositions

are chosen as evolved end-members, representing respectively the Low-Zr (500 ppm Ba, 600 ppm Zr and 35 ppm V) and the high-Zr (20 ppm Ba, 1200 ppm Zr and 30 ppm V) phonolitic units. The composition of these end-memebrs is represented by the average compositions pumice clasts ABP-F/PC2 and ABP-F/PC3. The feldspar composition used to plot the assimilation trend has a concentration of 5080 ppm Ba. The major and trace element compositions of all these end-member melts and whole rocks are listed in the Supplementary Material.

The distribution of glass chemical analyses on the different products (Ba, Sr and Eu enrichments dependent not on melt chemistry but on different juvenile products) suggests a variable combination of processes in the mixing event. The banded pumice and the mixed lapilli are consistent with a mixing and assimilation of an alkali feldspar-rich, low-Zr phonolite, suggesting that a significant amount of interstitial, low-Zr melt was present at the time of mixing. This crystal-rich reservoir may have been heated and partially melted before the interaction with the mafic magma. In contrast, the mafic scoria indicates mixing with a more heterogeneous reservoir, where a component of low-Zr and high-Zr phonolite was present in short scales. This suggests that the interface between the low-Zr and the high-Zr regions in the phonolitic body was disturbed by convection shortly before the eruption, likely in response to the intrusion of the mafic magma into the phonolitic chamber.

The results presented here combined with literature data can also shed some light on the origin of geochemical variability in the Las Cañadas edifice. Overall, the composition of eruptive products throughout the three explosive cycles of the Las Cañadas edifice (Ucanca, Guajara, and Diego Hernández) is markedly bimodal, with a large abundance of

basanites and tephrites on the mafic side, and phonolites on the evolved side, with a lesser number of intermediate compositions. A vast majority of these intermediate rocks are represented by banded pumices, and thus they cannot be considered as products of fractional crystallization but instead represent mixing between the two end-members (Olin, 2007). Such distributions are consistent with the intra-clast major and trace element distributions presented here, confirming that magma mixing, controlled by diffusive hybridization, can explain a significant portion of the variability of the DHF and is capable of leaving an important signature at a large scale.

Estimation of volume proportions of magmas in the El Abrigo eruption

Using an energy balance approach, some constrains can be placed on the relative proportions of tephritic and phonolitic magmas involved in the pre-eruptive mixing event of the El Abrigo eruption. Upon mixing between a hot, mafic magma coming from depth and a cooler, crystal-rich felsic magma stored in the crust, both magmas will experience a temperature variation up to eventually reaching an equilibrium. Following equations 2a and 2b in Folch and Marti (1998), the temperature variation of felsic (ΔT_m) and mafic (ΔT_m) magmas in contact with each other will be:

$$\Delta T_f = \frac{\varphi \rho_m C_m}{\varphi \rho_m C_m + \rho_f C_f} \left(T_{mi} - T_{fi}\right) \quad (1)$$

$$\Delta T_m = \frac{\rho_f C_f}{\varphi \rho_m C_m + \rho_f C_f} \left(T_{fi} - T_{mi}\right) \quad (2)$$

Where T_{mi} and T_{fi} are the initial temperatures of the mafic and felsic end-members, respectively; C_m and C_f are their heat capacities, and ρ_m and ρ_f, their densities. The φ

parameter represents the volume fraction of the mafic magma relative to the felsic one, i.e. $\varphi = V_m/V_f$.

The initial temperatures of the end-member magmas were taken as those obtained in from mineral thermobarometry, representing the storage temperature of the tephritic and phonolitic magmas immediately prior to the mixing event (that is, T_{mi} = 1050°C and T_{fi} = 890°C). Additionally, the storage temperature obtained by Andújar et al. (2008) was used for the phonolitic body (T_{fi} = 825°C). Specific capacities of magmas were calculated considering a phonolitic reservoir composed of 15 vol. % feldspar and 85 vol. % melt, and a tephritic magma with 15 vol. % amphibole, 10 vol. % clinopyroxene, 5 vol. % plagioclase and 70 vol % melt (see Supplementary Material). A water content of 3 wt.% was used for both melt phases.

According to the evidence obtained during the present work and literature data, the K-feldspar dominated phonolitic magma mush experienced some degree of melting either prior to or during magma interaction. Hence, the temperature of the phonolitic body must have been increased to the K-feldspar liquidus in the system. Thermodynamic calculations performed with rhyolite-Melts (Gualda et al., 2012) starting with a low-Zr phonolitic composition with 3 wt.% H_2O at a pressure of 130 MPa (Andújar et al, 2008) place the K-feldspar liquidus at 924°C.

Taking these data as input in the equations (1) and (2), we find that considering a T_{fi} = 890°C, we need a φ value of 0.25, equivalent to a 20 volume % proportion of mafic magma relative to phonolitic magma to increase its temperature to 924°C. On the other hand, taking a T_{fi} = 825°C as suggested by Andújar et al. (2008), the value of φ is increased to 0.75 (43 vol. % of injected mafic magma). Given that the proportions of

crystal-rich regions and crystal-poor regions in the phonolitic magma reservoir are not known, this calculation allows to place some reasonable first-order constraints in the mafic magma input immediately before the eruption. Moreover, these values agree with the proportion of mafic and banded juvenile clasts in the El Abrigo outcrops, as described by Pittari (2004).

The El Abrigo eruption plumbing system

A model for the pre-eruptive El Abrigo plumbing system is proposed based on the current work (data from this study and published data) **(Fig. 15**). Literature data suggest that the pre-mixing magma reservoir beneath Las Cañadas volcano at the end of the Diego Hernández cycle was zoned, with a crystal-rich cumulate zone at the bottom of the chamber and a crystal-poor phonolitic magma in the upper sector. The presence of abundant syenitic lithics suggests that the margins of the chamber were already crystallized, although these lithics could also have been incorporated from older plutons (Wolff et al., 2000). A storage temperature of 825ºC and a pressure of 130 MPa (depth of 4-5 km) were suggested for this magma reservoir (Andújar et al., 2008). Alkali-feldspars examined in this work suggest a temperature of 893 ± 9 ºC, hotter than estimates of Andújar et al., (2008). This discrepancy could be due to the presence of thermal gradients in the phonolitic chamber, with the alkali feldspar thermometry representing an upper, hotter portion of the system.

On the other hand, amphibole thermometry and clinopyroxene-melt thermo-barometry suggest that the tephritic end-member was stored at the base of the oceanic crust at 1050

ºC and 430 MPa, corresponding to a depth of 12-15 km. At these conditions, the mineral cargo was potentially in equilibrium with a phonotephritic melt phase with 51-53 wt% SiO_2, ca. 3-4 wt% MgO and water contents around 3 wt%. A pertinent question is the relationship between more primitive basanites and the tephrite/phonotephrite. We propose a combination of fractional crystallization from a parental basanite to produce tephrite, and subsequent mixing between tephrite and new basanitic batches as processes leading to the accumulation of the tephritic to phonotephritic end-member at the base of the curst. Fractional crystallization is supported by the distribution of literature whole-rock data in major element bivariate diagrams (especially P_2O_5, with a maximum at ca. 47 wt% likely related to the onset of apatite crystallization), and by rhyolite-MELTS (Gualda et al., 2012) thermodynamic modelling resulting in the LLOD plotted in **Fig. 14**. The presence of abundant plagioclase with sieve-textured cores hosting basanitic melt inclusions suggest that this deep reservoir was periodically replenished by the more primitive basanitic magma, leading to plagioclase resorption. In turn, ultimate ascent from this lower crustal reservoir could have been triggered by volatile accumulation and reduced density triggered by fractionation, a process recently proposed as a primary control of basalt chemistry in ocean island plumbing systems (Ubide et al., 2021).

Upon ascent, the tephritic magma encountered the shallow phonolitic magma chamber and intruded into it, first interacting with the mush/cumulate zone and triggering its melting and partial assimilation. Subsequently, lesser portions of the mafic magma could have interacted and mixed with the crystal-poor, more evolved phonolite in the top of the reservoir. Magma hybridization was greatly aided by the high-water contents present in both end-members, which reduced viscosity contrasts and enhanced diffusive chemical

exchange. At the same time, the high volatile concentrations probably enhanced the explosive potential. The *cpx* microlites ubiquitously found in the mafic domains could have grown either during the ascent of the tephrite magma or during mixing in the phonolitic reservoir, given its initial equilibrium with the hosting melt.

In this view, magma mixing/replenishment occurred not only at the uppermost part of the plumbing system but also played a significant role in the genesis of the tephrite end-member at lower crustal levels. Therefore, a mixture of processes operating at the same time at different crustal levels can be envisaged (basanite-tephrite-phonolite differentiation, mixing between these reservoirs, and crystal mush/cumulate disruption). This multistage structure of the El Abrigo plumbing system agrees with previous findings on differentiation processes in the Canary Islands (Freundt-Malecha et al., 2001; Klugel et al. 2005), also proposed for Tenerife by Ablay et al. (1998) and Sliwinski et al. (2015).

SUMMARY AND CONCLUSIONS

The intricate texture and geochemistry of diverse products from the El Abrigo member, coupled to intensive variables extracted from mineral and mineral-melt equilibria, depict complex pre-eruptive dynamics in the magmatic system below Tenerife at the end of the Diego Hernandez cycle. Here we have shown that:

1. Glass geochemistry traced by major and trace element distribution shows that magma mixing immediately before the El Abrigo eruption was complex and involved a less evolved tephritic magma and a zoned phonolitic magma reservoir, with three end-members interacting between them.

2. According to thermobarometric results, the tephritic end-member evolved at or near the Moho below the island at pressures around 360-400 MPa and temperature of 1050°C, where it was periodically replenished by more primitive basanite.
3. Magmas involved in the El Abrigo system were water-rich, with water contents of the order of 3 wt% for the tephrite, likely increasing to 4 wt% in the phonolitic magma reservoir.
4. The magma mixing event involved overall proportions of tephritic magma between 20 and 43 vol. % and occurred shortly (in the order of hours to few days) before the onset of the eruption.

SUPPLEMENTARY DATA

The data underlying this article are available in its online Supplementary Materials at Journal of Petrology Online.

FUNDING

This work was supported by a co-financed postdoctoral grant ("*Assegno di Ricerca*") from the University of Turin and the Ludwig Maximilian University of Munich to D.G.G. and by the European Research Council Consolidator Grant ERC-2013-CoG 612776 (CHRONOS) to D.P. Sampling was carried out by D.P and J.P.M. in the frame of VERTIGO Initial Training Network (FP7-People-2013-ITN 607905), funded by the 7th

Framework Programme of the European Union. D.G.G also acknowledges the Alexander von Humboldt Foundation for a postdoctoral fellowship at the Leibniz University of Hannover. J.V. and D.B.D. wish to acknowledge the support of ERC Advanced Grant 834255 (EAVESDROP).

ACKNOWLEDGEMENTS

We are grateful to Kathrin Laeger (University of Perugia) for sample collection, Carmelo Sibio (University of Turin) and Hilger Lohringer (LMU Munich) for sample preparation, and Dirk Muller (LMU Munich), Roberto Cossio and Simona Ferrando (University of Turin) for assistance with EPMA, SEM and Raman spectroscopy, respectively. Filippo Ridolfi (Leibniz Universität Hannover) is acknowledged for helpful discussion on amphibole thermobarometry. This manuscript has been improved significantly by thorough and constructive reviews from Ewa Słaby, Jakub Sliwinski and an anonymous referee. We also thank Georg Zellmer and Madeleine Humphreys for the editorial handling of the manuscript.

REFERENCES

Ablay, G., Carroll, M., Palmer, M., Martí, J. & Sparks, R. (1998). Basanite-phonolite lineages of the Teide-Pico Viejo volcanic complex, Tenerife, Canary Islands. *Journal of Petrology* **39**, 905-936.

Adam, J. & Green. T. (2006). Trace element partitioning between mica- and amphibole-bearing garnet lherzolite and hydrous basanitic melt: 1. Experimental results and the investigation of controls on partitioning behaviour. *Contributions to Mineralogy and Petrology* **152**, 1-17.

Ancochea, E., Fuster, J.M., Ibarrola, E., Cendrero, A., Coello, J., Hernan, F., Cantagrel, J.M. & Jamond, C. (1990). Volcanic evolution of the island of Tenerife (Canary Islands) in the light of new K-Ar data. *Journal of Volcanology and Geothermal Research* **44** (3-4), 231-249.

Ancochea, E., Huertas, M.J., Cantagrel, J.M., Coello, J. & Fúster, J.M. (1999). Evolution of the Las Cañadas edifice and its implications for the origin of the Cañadas Caldera (Tenerife, Canary Islands). *Journal of Volcanology and Geothermal Research* **88** (3), 177-199.

Andújar, J., Costa, F., Martí, J., Wolff, J.A. & Carroll, M.R. (2008). Experimental constraints on pre-eruptive conditions of phonolitic magma from the caldera-forming El Abrigo eruption, Tenerife (Canary Islands). *Chemical Geology* **257**, 173-191.

Araña, V., Martí, J., Aparicio, A., García-Cacho, L. & García-García, R. (1994). Magma mixing in alkaline magmas: An example from Tenerife, Canary Islands. *Lithos* **32**, 1-19.

Bachmann, O. & Bergantz, G.W. (2003). Rejuvenation of the Fish Canyon magma body: a window into the evolution of large volume silicic magma systems. *Geology* **31** (9), 789-792.

Bain, A.A., Jellinek, A.M. & Wiebe, R.A. (2013). Quantitative field constraints on the dynamics of silicic magma chamber rejuvenation and overturn. *Contributions to Mineralogy and Petrology* **165**, 1275-1294.

Beier, C., Haase, K.M. & Hansteen, T.H. (2006). Magma evolution of the Sete Cidades Volcano, Sao Miguel, Azores. *Journal of Petrology* **47**, 1375–1411.

Bindeman, I., Davis, A.M. & Drake, M.J. (1998). Ion microprobe study of plagioclase-basalt partition experiments at natural concentration levels of trace elements. Geochimica et Cosmochimica Acta **62** (7), 1175-1193.

Brown, R.J., Barry, T.L., Branney, M.J., Pringle, M.S. & Bryan, S.E. (2003) The Quaternary pyroclastic succession of southeast Tenerife, Canary Islands: explosive eruptions, related caldera subsidence, and sector collapse. *Geological Magazine* **140** (3), 265-288.

Bryan, S.E. (2006). Petrology and geochemistry of the quaternary caldera-forming, phonolitic Granadilla eruption, Tenerife (Canary Islands). *Journal of Petrology* **47** (8), 1557-1589. doi: 10.1093/petrology/egl020

Bryan, S.E., Martí, J. & Cas, R..A.F. (1998). Stratigraphy of the Bandas del Sur Formation: an extracaldera record of Quaternary phonolitic explosive eruptions from the Las Cañadas edifice, Tenerife (Canary Islands). *Geological Magazine* **135**, 605-636.

Bryan, S.E., Martí, J. & Leosson, M. (2002). Petrology and geochemistry of the Bandas del Sur Formation, Las Cañadas edifice, Tenerife (Canary Islands). *Journal of Petrology* **43** (10), 1815-1856.

Chamberlain, K.J., Barclay, J., Preece, K., Brown, R.J., McIntosh, I. & EIMF (2020). Deep and disturbed: conditions for formation and eruption of a mingled rhyolite at Ascension Island, south Atlantic. *Volcanica* **3** (1), 139-153.

Chakraborty S., Dingwell D. B. & Rubie D. C. (1995), Multicomponent diffusion in ternary silicate melts in the system K_2O-Al_2O_3-SiO_2: II. Mechanisms, systematics, and geological applications. *Geochimica et Cosmochimica Acta* **59**, 265–277.

Clague, D.A. (1978). The oceanic basalt-trachyte association: an explanation fo the Daly gap. *The Journal of Geology* **86**, 739-743.

Daly, R.A. (1925). The geology of Ascension island. *Proceedings of the American Academy of Arts and Sciences* **60**, 3-80.

De Campos, C.P., Dingwell, D.B., Perugini, D., Civetta, L. & Fehr, T.K. (2008). Heterogeneities in magma chambers: Insights from the behavior of major and minor elements during mixing experiments with natural alkaline melts. *Chemical Geology* **256**, 131-145.

DeVitre, C., Gazel, E., Allison, C.M., Soto, G., Madrigal., P., Alvarado, G. & Lücke, O.H. (2019). Multi-stage chaotic magma mixing at Turrialba volcano. *Journal of Volcanology and Geothermal Research* **381**, 330-346.

Edgar, C.J., Wolff, J.A., Nichols, H.J., Cas, R.A.F. & Marti, J., (2002). A complex Quaternary ignimbrite-forming phonolitic eruption: the Poris member of the Diego Hernández Formation (Tenerife, Canary Islands). *Journal of Volcanology and Geothermal Research* **118**, 99-130.

Edgar, C.J., Wolff, J.A., Olin, P.H., Nichols, H.J., Pittari, A., Cas, R.A.F., Reiners, P.W., Spell, T.L. & Martí, J. (2007). The late Quaternary Diego Hernández formation,

Tenerife: Volcanology of a complex cycle of voluminous explosive phonolitic eruptions. *Journal of Volcanology and Geothermal Research* **160**, 59-85.

Eichelberger, J.C. & Izbekov, P.E. (2000). Eruption of andesite triggered by dyke injection: contrasting cases at Karymsky Volcano, Kamchatka and Mt Katmai, Alaska. *Philosophical Transactions of the Royal Society A* **358** (1770), 1465-1485.

Erdmann, S., Martel, C., Pichavant, M., Kushnir, A. (2014). Amphibole as an archivist of magmatic crystallization conditions: problems, potential, and implications for inferring magma storage prior to the paroxysmal 2010 eruption of Mount Merapi, Indonesia. *Contributions to Mineralogy and Petrology* **167**, 1016.

Folch, A. & Martí, J. (1998). The generation of overpressure in felsic magma chambers by replenishment. *Earth and Planetary Science Letters* **163**, 301-314.

Freundt, A. & Schminke, H.-U. (1992) Mixing of rhyolite, trachyte and basalt magma erupted from a vertically and laterally zoned reservoir, composite flow P1, Gran Canaria. *Contributions to Mineralogy and Petrology* **112**, 1-19.

Freundt-Malecha, B., Schmincke, H.-U. & Freundt, A. (2001). Plutonic rocks of intermediate composition on Gran Canaria: the missing link of the bimodal volcanic rock suite. *Contributions to Mineralogy and Petrology* **141**, 430-445.

Geldmacher, J., Hoernle, K., Van der Bogaard, P., Duggen, S. & Werner, R. (2005). New Ar-40/Ar39 age and geochemical data from seamounts in the Canary and Madeira volcanic provinces: support for the mantle plume hypothesis. *Earth and Planetary Science Letters* **237**, 85-101.

Giordano D., Romano C. & Dingwell D.B. (2000). Viscosity of a Teide phonolite in the welding interval. *Journal of Volcanology and Geothermal Research* **103**, 239-245.

Giordano D., Nichols A.R.L. & Dingwell D.B. (2005). Glass transition temperatures of natural hydrous melts: a relationship with shear viscosity and implications for the welding process. *Journal of Volcanology and Geothermal Research* **142**, 105-118.

González, P.J., Samsonov, S.V., Pepe, S., Tiampo, K.F., Tizzani, P., Casu, F., Fernández, J., Camacho, A.G. & Sansosti, E. (2013). Magma storage and migration associated with the 2011–2012 El Hierro eruption: Implications for crustal magmatic systems at oceanic island volcanoes. *Journal of Geophysical research Solid Earth* **118** (8), 4361-4377.

González-García, D., Behrens, H., Petrelli, M., Vetere, F., Morgavi, D., Zhang, C. & Perugini, D. (2017). Water-enhanced interdiffusion of major elements between natural shoshonite and high-K rhyolite melts. *Chemical Geology* **466**, 86-101.

González-García, D., Petrelli, M., Behrens, H., Vetere, F., Fischer, L.A., Morgavi, D., & Perugini, D. (2018). Diffusive exchange of trace elements between alkaline melts: implications for element fractionation and timescale estimations during magma mixing. *Geochimica et Cosmochimica Acta* **233**, 95-114.

Gualda, G.A.R., Ghiorso, M.S., Lemmons, R.V. & Carley, T.L. (2012). Rhyolite-MELTS: A modified calibration of MELTS optimized for silica-rich, fluid bearing magmatic systems. *Journal of Petrology* **53**, 875-890.

Guillou, H., Carracedo, J.C., Paris, R. & Perez Torrado, F.J. (2004). Implications for the early shield-stage evolution of Tenerife from K/Ar ages and magnetic stratigraphy. *Earth and Planetary Science Letters* **222** (2), 599-614.

Helz, R.T., Clague, D.A., Mastin, L.G. & Rose, T.R. (2014). Electron microprobe analyses of glasses from Kilauea Tephra Units, Kilauea volcano, Hawaii. U.S. Geological Survey Open File Report 2014-1090, 24p.

Huertas, M.J., Arnaud, N.O., Ancochea, E., Cantagrel, J.M. & Fúster, J.M. (2002). Ar-40/Ar-39 stratigraphy of pyroclastic units from the Las Cañadas volcanic edifice (Tenerife, Canary Islands) and their bearing on the structural evolution. *Journal of Volcanology and Geothermal Research* **115**, 351-365.

Hunt, J.E., Cassidy, M. & Talling, P.J. (2018). Multi-stage volcanic island flank collapses with coeval explosive caldera-forming eruptions. *Scientific Reports* **8**, 1146.

Iacovino, K., Oppenheimer, C., Scaillet, B., & Kyle, P. (2016). Storage and evolution of mafic and intermediate alkaline magmas beneath Ross Island, Antarctica. Journal of Petrology 57, 93-118.

Jarosewich, E., Nelen, J.A. & Norberg, J.A. (1980). Reference samples for Electron Microprobe Analysis. *Geostandards Newsletter* **4**, 43-47.

Jeffery, A.J. & Gertisser, R. (2018). Peralkaline Felsic Magmatism of the Atlantic Islands, *Frontiers in Earth Sciences* **6**, 145.

Kress V. C. & Ghiorso M. S. (2004). Thermodynamic modeling of post-entrapment crystallization in igneous phases. *Journal of Volcanology and Geothermal Research* **137**, 247–260.

Klügel, A., Hansteen. T.H. & Galipp, K. (2005). Magma storage and underplating beneath Cumbre Vieja volcano, La Palma (Canary Islands). *Earth and Planetary Science Letters* **236**, 211-226.

Laeger, K., Petrelli, M., Andronico, D., Misiti, V., Scarlato, P., Cimarelli, C., Taddeucci, J., Del Bello, E. & Perugini, D. (2017). High-resolution geochemistry of volcanic ash highlights complex magma dynamics during the Eyjafjallajökull 2010 eruption. *American Mineralogist* **102**, 1173-1186.

Laeger, K., Petrelli, M., Morgavi, D., Lustrino, M., Pimentel, A., Paredes-Mariño, J., Astbury, R.L., Kuppers, U., Porreca, M. & Perugini, D. (2019). Pre-eruptive conditions and triggering mechanism of the ˜16ka Santa Bárbara explosive eruption of Sete Cidades Volcano (São Miguel, Azores). *Contributions to Mineralogy and Petrology* **174**, 11.

Larsen, L.M. (1979). Distribution of REE and other trace elements between phenocrysts and peralkaline undersaturated magmas, exemplified by rocks from the Gardar igneous province, south Greenland. *Lithos* **12**, 303-315.

Le Losq, C., Neuville, D.R., Moretti, R. & Roux, J. (2012). Determination of water content in silicate glasses using Raman spectroscopy: Implications for the study of explosive volcanism. *American Mineralogist* **97**, 779-790.

Leonard, G.S., Cole, J.W., Naim, I.A. & Sell, S. (2002). Basalt triggering of the c. AD 1305 Kaharoa rhyolite eruption, Tarawera Volcanic Complex, New Zealand. *Journal of Volcanology and Geothermal Research* **115**, 461-486.

Lodge, A., Nippress, S.E.J., Rietbrock, A., García-Yeguas, A. & Ibáñez, J.M. (2012). Evidence for magmatic underplating and partial melt beneath the Canary Islands derived using teleseismic receiver functions. *Physics of the Earth and Planetary Interiors* **212-213**, 44-54.

Longpré, M.-A., Troll, V.R., Walter, T.R. & Hansteen, T.H. (2009). Volcanic and geochemical evolution of the Teno Massif, Tenerife, Canary Islands: some repercussions of giant landslides on ocean island magmatism. *Geochemistry, Geophysics, Geosystems* **10**, Q12017.

Martí, J. (2019). Las Cañadas caldera, Tenerife, Canary Islands: A review, or the end of a long volcanological controversy. *Earth-Science Reviews* **196**, 102889.

Martí, J.& Gudmundsson, A. (2000) The Las Cañadas caldera (Tenerife, Canary Islands): an overlapping collapse caldera generated by magma-chamber migration. *Journal of Volcanology and Geothermal Research* **103**, 161-173.

Marti, J., Mitjavila, J. & Araña, V. (1994). Stratigraphy, structure and geochronology of the Las Cañadas Caldera (Tenerife, Canary Islands). *Geological Magazine* **131**, 715-727.

Marti, J., Hurlimann, M., Ablay, G.J. & Gudmundsson, A. (1997). Vertical and lateral collapses in Tenerife (Canary Islands) and other volcanic ocean islands. *Geology* **25**, 879-882.

Martí, J., Zafrilla, S., Andújar, J., Jiménez-Mejias, M., Scaillet, B., Pedrazzi, D., Doronzo, D. & Scaillet, S. (2020). Controls of magma chamber zonation on eruption dynamics and deposits stratigraphy: The case of El Palomar fallout succession (Tenerife, Canary Islands). *Journal of Volcanology and Geothermal Research* **399**, 106908.

Martinez-Arevalo. C., Mancilla, F.D.L., Helffrich, G. & Garcia, A. (2013). Seismic evidence of a regional sublithospheric low velocity layer beneath the Canary Islands. *Tectonophysics* **608**, 568-599.

Masotta, M., Mollo, S., Freda, C., Gaeta, M. & Moore, G. (2013). Clinopyroxene-liquid thermometers and barometers specific to alkaline differentiated magmas. *Contributions to Mineralogy and Petrology* **166**, 1545-1561.

Mollo, S., Masotta, M., Forni, F., Bachmann, O., De Astis, G., Moore, G. & Scarlato, P. (2015). A K-feldspar-liquid hygrometer specific to alkaline differentiated magmas. *Chemical Geology* **392**, 1-8.

Montagna, C. P., Papale, P. & Longo, A. (2015). Timescales of mingling in shallow magmatic reservoirs. In: Caricchi, L. & Blundy, J. D. (eds). Chemical, Physical and Temporal Evolution of Magmatic Systems. *Geological Society, London, Special Publications* **422**, 131-140.

Morgavi, D., Perugini, D., De Campos, C.P., Ertel-Ingrisch, W., Lavallee, Y., Morgan, L. & Dingwell, D.B. (2013). Interactions between rhyolitic and basaltic melts unravelled by chaotic mixing experiments. *Chemical Geology* **346**, 199-212.

Morgavi D., Arzilli F., Pritchard C., Perugini D., Mancini L., Larson P. & Dingwell D.B., (2016). The Grizzly Lake complex (Yellowstone Volcano, USA): Mixing between basalt and rhyolite unravelled by microanalysis and X-ray microtomography. *Lithos* **260**, 457-474.

Morgavi, D., Arienzo, I., Montagna, C., Perugini, D. & Dingwell, D.B. (2017). Magma mixing: History and dynamics of an eruption trigger. In: Joachim Gottsmann J., Neuberg, J. & Scheu., B. (eds.) *Volcanic Unrest - From Science to Society*. Springer International Publishing, 123-137.

Nichols, H. J., 2001. Petrologic and Geochemical Variation of a Caldera-Forming Ignimbrite: the Abrigo Member, Diego Hernández Formation, Tenerife, Canary

Islands (Spain). MSc Thesis, Department of Geology, Washington State University, Pullman, 123 pp.

Neave, D.A., Hartley, M.E., Maclennan, J., Edmonds, M. & Thordarson, T. (2017). Volatile and light litophile elements in high anorthite plagioclase-hosted melt inclusions from Iceland. *Geochimica et Cosmochimica Acta* **205**, 100-118.

Neumann, E.-R., Wulff-Pedersen, E., Simonsen, S.L., Pearson, N.J., Martí, J. & Mitjavila, J. (1999). Evidence for Fractional Crystallization of Periodically Refilled Magma Chambers in Tenerife, Canary Islands. *Journal of Petrology* **40** (7), 1089-1123.

Oglialoro, E., Frezzotti, M.L., Ferrando, S., Tiraboschi, C., Principe, C., Groppelli, G. & Villa, I.M. (2017). Lithospheric magma dynamics beneath the El Hierro Volcano, Canary Islands: insights from fluid inclusions. *Bulletin of Volcanology* **79**, 70.

Olin, P.H. Magma dynamics of the phonolitic Diego Hernández Formation, Tenerife, Canary Islands (2007). PhD Thesis, Washington State University, 416 pp.

Paredes-Mariño, J., Dobson, K.J., Ortenzo, G., Kueppers, U., Morgavi, D., Petrelli, M., Hess, K.-U., Laeger, K., Porreca, M., Pimentel., A. & Perugini, D. (2017). Enhancement of eruption explosivity by heterogeneous bubble nucleation triggered by magma mingling. *Scientific Reports* **7**, 16897.

Paton C., Hellstrom J., Paul B., Woodhead J. & Hergt J. (2011). Iolite: freeware for the visualization and processing of mass spectrometric data. *Journal of Analytical Atomic Spectrometry* **26**, 2508–2518.

Pearce N. J. G., Perkins W. T., Westgate J. A., Gorton M. P., Jackson S. E., Neal C. R. & Chenery S. P. (1997). A compilation of new and published major and trace element

data for NIST SRM 610 and NIST SRM 612 glass reference materials. *Geostandards Newsletter* **21**, 115–144.

Perugini, D., Poli, G. & Marzuoli, R. (2003). Chaotic advection, fractals and diffusion during mixing of magmas: evidence from lava flows. *Journal of Volcanology and Geothermal Research* **124**, 255-279.

Perugini, D., De Campos, C.P., Dingwell, D.B., Petrelli, M. & Poli, G. (2008). Trace element mobility during magma mixing: Preliminary experimental results. *Chemical Geology* **256**, 146-157.

Perugini, D., De Campos, C.P., Petrelli, M. & Dingwell, D.B. (2015). Concentration variance decay during magma mixing: a volcanic chronometer, *Scientific Reports* **5**, 14225.

Perugini, D., Poli, G., Petrelli, M., De Campos, C.P. & Dingwell, D.B. (2010). Time-scales of recent Phlegrean Fields eruptions inferred from the application of a 'diffusive fractionation' model of trace elements. *Bulletin of Volcanology* **72**, 431-447.

Petrelli M., Morgavi D., Vetere F. & Perugini D. (2016a). Elemental imaging and petro-volcanological applications of an improved Laser Ablation Inductively Coupled Quadrupole Plasma Mass Spectrometry. *Periodico di Mineralogia* **85**, 25–39.

Petrelli M., Laeger K. & Perugini D. (2016b). High resolution trace element determination of geological samples by laser ablation quadrupole plasma mass spectrometry: implications for glass analysis in volcanic products. *Geosciences Journal* **20** (6), 851–863.

Pittari, A. (2004). Eruption dynamics and emplacement processes for the climactic Abrigo Member, Tenerife, Canary Islands. PhD Thesis, Monash University, Australia, 327pp.

Pittari, A., Cas, R.A.F. & Marti, J. (2005). The occurrence and origin of prominent massive, pumice-rich ignimbrite lobes within the Late Pleistocene Abrigo Ignimbrite, Tenerife, Canary Islands. *Journal of Volcanology and Geothermal Research* **139**, 271-293.

Pittari, A., Cas, R.A.F., Edgar, C.J., Nichols, H.J., Wolff, J.A. & Martí, J. (2006). The influence of paleotopography on facies architecture and pyroclastic flow processes of a lithic-rich ignimbrite in a high gradient setting: the Abrigo ignimbrite, Tenerife, Canary Islands. *Journal of Volcanology and Geothermal Research* **152**, 273-315.

Putirka, K.D. (2008). Thermometers and barometers for igneous systems. *Reviews in Mineralogy and Geochemistry* **69**, 61-120.

Putirka, K. (2016). Amphibole thermometers and barometers for igneous systems and some implications for eruption mechanisms of felsic magmas at arc volcanoes. *American Mineralogist* **101** (4), 841-858.

Ridolfi, F. (2021). Amp-TB2: An updated model for calcic amphibole thermobarometry. *Minerals* **11**, 324.

Ridolfi, F. & Renzulli, A. (2012). Calcic amphiboles in calc-alkaline and alkaline magmas: thermobarometric and chemometric empirical equations valid up to 1,130 ºC and 2.2 GPa. *Contributions to Mineralogy and Petrology* **163**, 877-895.

Ridolfi, F., Zanetti, A., Renzulli, A., Perugini, D., Holtz, F. & Oberti, R. (2018). AMFORM, a new mass-based model for the calculation of the unit formula of

amphiboles from electron microprobe analyses. *American Mineralogist* **103**, 1112–1125.

Rossi, S., Petrelli, M., Morgavi, D., Vetere, F.P., Almeev, R.R., Astbury, R.L. & Perugini, D. (2019). Role of magma mixing in the pre-eruptive dynamics of the Aeolian Islands volcanoes (Southern Tyrrhenian Sea, Italy). *Lithos* **324-325**, 165-179.

Schmidt, M.W., Weidendorfer, D. (2018). Carbonatites in oceanic hotspots. *Geology* **46**, 435-438.

Seligman, A.N., Bindeman, I.N., Watkins, J.M. & Ross, A.M. (2016). Water in volcanic glass: From volcanic degassing to secondary hydration. *Geochimica et Cosmochimica Acta* **191**, 216-238.

Self, S. (1992). Krakatau revisited: the course of events and interpretation of the 1883 eruption. *GeoJournal* **28** (2), 109-121.

Shea, T., Hellerbrand, E., Gurioli, L. & Tuffen, H. (2014). Conduit- to localized-scale degassing during plinian eruptions: Insights from major Element and volatile (Cl and H_2O) analyses within Vesuvius AD 79 pumice. *Journal of Petrology* **55**, 315-344.

Sigmarsson, O., Vlastelic, I., Andreasen, R., Bindeman, I., Devidal, J.-L., Moune, S., Keiding, J.K., Larsen, G., Höskuldsson, A. & Thordarson, T. (2011) Remobilization of silicic intrusion by mafic magmas during the 2010 Eyjafjallajökull eruption. *Solid Earth* **2**, 271–281.

Sigmundsson, F., Hreinsdóttir, S., Hooper, A., Árnadóttir, T., Pedersen, R., Roberts, M.J., Óskarsson, N., Auriac, A., Decriem, J., Einarsson, P., Geirsson, H., Hensch, M.,

Ófeigsson, B.G., Sturkell, E., Sveinbjörnsson, H. & Feigl, K.L. (2010). Intrusion triggering of the 2010 Eyjafjallajökull eruption. *Nature* **468**, 426–430.

Sliwinski, J.T., Bachmann, O., Ellis, B.S., Dávila-Harris, P., Nelson, B.K. & Difel, J. (2015). Eruption of shallow crystal cumulates during explosive phonolitic eruptions on Tenerife, Canary Islands. *Journal of Petrology* **56** (11), 2173-2194.

Sliwinski, J.T., Ellis, B.S., Dávila-Harris, P., Wolff, J.A., Olin, P.H., Bachmann, O. (2017). The use of biotite trace element compositions for fingerprinting magma batches at Las Cañadas volcano, Tenerife. *Bulletin of Volcanology* **79**, 1, 1-15.

Sparks, S.R.J., Sigurdsson, H. & Wilson, L. (1977). Magma mixing: a mechanism for triggering acid explosive eruptions. *Nature* **267**, 315-318.

Stroncik, N.A., Klügel, A. & Hansteen, T.H. (2009). The magmatic plumbing system beneath El Hierro (Canary Islands): constraints from phenocrysts and naturally quenched basaltic glasses in submarine rocks. *Contributions to Mineralogy and Petrology* **157**, 593-607.

Turnbull, R., Weaver, S., Tulloch, A., Cole, J., Handler, M. & Ireland, T. (2010). Field and geochemical constraints on mafic-felsic interactions, and processes in high-level arc magma chambers: an example from the Halfmoon pluton, New Zealand. *Journal of Petrology* **51**, 1477-1505.

Ubide, T., Larrea, P., Becerril, L., & Galé, C. (2021). Volcanic plumbing filters on ocean-island basalt geochemistry. *Geology* **49**, 1-6.

Villemant, B., Jaffrezic, H., Joron, J.-L. & Treuil, M. (1981). Distribution coefficients of major and trace elements; fractional crystallization in the alkali basalt series of

Chaîne des Puys (massif Central, France). Geochimica et Cosmochimica Acta 45, 1997-2016.

Walter, T.R., Troll, V.R., Cailleau, B., Belousov, A. & Schminke H.-U. (2005). Rift zone reorganization through flank instability in ocean island volcanoes: an example from Tenerife, Canary Islands. *Bulletin of Volcanology* **67**, 281-291.

Waters, L.E. & Lange, R.A. (2015). An updated calibration of the plagioclase-liquid hygrometer-thermometer applicable to basalts through rhyolites. *American Mineralogist* **100**, 2172-2184.

Wiesmaier, S., Deegan, F.M., Troll, V.R., Carracedo, J.C., Chadwick, J.P. & Chew, D.M. (2011). Magma mixing in the 1100 AD Montaña Reventada composite lava flow, Tenerife, Canary Islands: interaction between rift zone and central volcano plumbing systems. *Contributions to Mineralogy and Petrology* **162**, 651-699.

Wilson S.A. (1997). The collection, preparation and testing of USGS reference material BCR-2G, 557 Columbia River Basalt. US Geological Survey Open File Report 98.

Wolff, J.A. (1985). Zonation, mixing and eruption of silica-undersaturated alkaline magma: a case study from Tenerife, Canary Islands. *Geological Magazine* **122** (6), 623-640.

Wolff, J.A., Grandy, J.S. & Larson, P.B. (2000). Interaction of mantle-derived magma with island crust? Trace element and oxygen isotope data from the Diego Hernandez Formation, Las Cañadas, Tenerife. *Journal of Volcanology and Geothermal Research* **103**, 346-366.

Wolff, J.A., Ellis, B.S., Ramos, F.C., Starkel, W.A., Boroughs, S., Olin, P.H. & Bachmann, O. (2015). Remelting of cumulates as a process for producing chemical

zoning in silicic tuffs: A comparison of cool, wet and hot, dry rhyolitic magma systems. *Lithos* **236-237**, 275-286.

Wolff, J.A., Forni, F., Ellis, B.S. & Szymanowski, D. (2020). Europium and barium enrichments in compositionally zoned felsic tuffs: A smoking gun for the origin of chemical and physical gradients by cumulate melting. *Earth and Planetary Science Letters* **540**, 116251.

Zhang, Y., Ni, H. & Chen, Y. (2010). Diffusion data in silicate melts, in: Zhang, Y., Cherniak, D.J. (Eds.). Diffusion in Minerals and Melts. *Reviews in Mineralogy and Geochemistry* **72**, 311-408.

FIGURE CAPTIONS

Fig. 1. Simplified geological map of Tenerife, including the current distribution of the DHF outcrops (red) and source area of the El Abrigo eruption in the north-eastern end of the Las Cañadas caldera (star). The sampling location is indicated. Modified from Martí et al. (2020); DHF distribution and vent location from Edgar et al. (2007).

Fig. 2. Different types of products from El Abrigo ignimbrite deposit studied here. **(a)** Typical white-greenish, highly porous, fibrous, aphyric phonolitic pumice. **(b, c)** Banded pumices with variable proportions of mafic and felsic domains ranging from strictly banded to convoluted structures. **(d)** Mafic scoria with numerous greenish phonolitic enclaves, slightly grading to banded in the right side. All pumices are embedded in a lithic-rich lapilli tuff visible in panels (b) and (c).

Fig. 3. Optical photomicrographs of banded pumices and black scoriae. (a) Kaersutite (*krs*) and plagioclase (*pl*) phenocrysts, the latter showing a core with sieve texture, embedded in a mafic scoria with phonolitic enclaves (bottom center). (b) Plagioclase with melt embayments containing brown glass. (c) Microscale banding in a banded pumice. (d) detail of a phonolitic enclave with complex mixing structures. (e) Narrow filament of hybrid glass (arrows) inside a phonolitic enclave. (f) Small-scale inhomogeneities in hybrid glasses.

Fig. 4. Selected back-scattered electron images (BSE) of the composite Abrigo products. **(a)** Phonolitic enclave inside a black scoria. **(b)** Detail of a banded pumice with white and dark domains indicated. **(c)** Complex contact between phonolitic and mafic glass in a banded pumice, **(d)** a phonolitic enclave and **(e)** a lapilli-sized, crystal-free mixed clast.

(f) High-resolution image of a black scoria. Yellow dots indicate microprobe analyses, and numbers are SiO_2 contents recalculated in anhydrous basis (wt%). Dashed line in (d) indicates the location of a glass transect. Minerals are kaersutite (*krs*), clinopyroxene (*cpx*), plagioclase (*pl*), K-feldspar (*kfs*), magnetite (*mag*), apatite (*ap*) and biotite (*bt*).

Fig. 5. Mineral chemistry of the El Abrigo composite products. **(a)** feldspar ternary diagram; **(b)** pyroxene quadrilateral (above) and chemical discrimination between phenocrysts and microlites (below); **(c)** Amphibole classification diagram, and **(d)** magnetite, with fields based in data from Bryan et al. (2002).

Fig. 6. Chemistry of glasses in mixed products, phonolitic pumices and plagioclase-hosted melt inclusions (this work) and selected whole-rock compositions of mafic and phonolitic products of the El Abrigo ignimbrite and basaltic rocks the Diego Hernández Formation (DHF). Melt inclusions have been corrected for post-entrapment crystallization (PEC). Data from [1] Pittari (2004), [2] Nichols (2001), [3] Sliwinski et al., 2015; [4] Bryan et al. (2002), [5] Wolff et al. (2000) and [6] Neumann et al. (1999).

Fig. 7. Major element variation diagrams of the El Abrigo glasses (this work) and related whole-rock compositions from literature. Plagioclase-hosted melt inclusions have been corrected for post-entrapment crystallization (red dots). Symbols and literature data as in **Fig. 6**.

Fig. 8. Selected trace element variation diagrams of the El Abrigo glasses and related whole-rock compositions, highlighting different inferred processes. Panels (a) and (b) show the enrichment in Ba and Eu in mafic to intermediate glasses, indicative of interaction and assimilation of an alkali feldspar-rich mush by the incoming mafic magma. LZ = low-Zr phonolite; HZ = high-Zr phonolite. Panels (c) and (d) show the

extent of mixing between a mafic precursor and two different phonolitic reservoirs. Symbols and literature data as in **Fig. 6**.

Fig. 9. Trace element spider diagrams normalized to ocean island basalt (OIB; Sun and McDonough, 1989), of (a) White pumices, (b) banded pumice, (c) mafic pumice with enclaves and (d) mixed lapilli clast. Spectra are colour coded according to Zr (panel a) and SiO_2 (panels b-d) concentrations.

Fig. 10. Distribution of H_2O concentrations in El Abrigo pumices, obtained following the Raman spectroscopic method of Le Losq (2012) as detailed in the Supplementary Material.

Fig. 11. Thermobarometric estimations for different mineral and mineral-melt equilibria in the composite eruption products. Calculations used are from [1] Masotta et al. (2013), [2] Ridolfi et al. (2012), and [3] Putirka (2008). For comparison, phonolite storage conditions inferred by [4] Andujar et al. (2008) are also plotted (825 ± 50°C, 130 ± 50 MPa). Inset: Rhodes diagram illustrating equilibrium conditions between clinopyroxene phenocrysts and the phonotephritic melt PT51 (see text). The equilibrium curve represents a $K_D(Fe\text{-}Mg)^{cpx/melt}$ of 0.28 ± 0.08 (Putirka, 2008). An H_2O content in melt of 3 wt% was used for clinopyroxene and plagioclase calculations. Kaersutite, clinopyroxene and plagioclase phenocrysts indicate pre-mixing conditions of the mafic endmembers, while alkali feldspars are indicative of those of the phonolitic reservoir.

Fig. 12. Major element SEM compositional maps of magma interaction in a banded pumice (same field as figure 4d) for (a) Si, (b) Mg and (c) Na, coupled to compositional histograms representing EPMA data of all composite pumices, with white pumices plotted as reference. Note how for Si and Mg, the mode of compositions in the mixed

products is coincident with the mode in white pumices, whilst it is not the case for Na distribution.

Fig. 13. Selected EPMA and LA-ICP-MS compositional profiles traversing mafic filaments in phonolitic enclaves of the mafic scoria sample. The extent of the mafic filaments is marked as grey bands. Thin filaments are more hybridized than thick filaments, some of which show gradational contact.

Fig. 14. Zr-Ba-10×V triangular diagram summarising the different interactions between mafic and felsic reservoirs occurring in the El Abrigo eruption. The mafic endmember has been chosen as the DHF tephrite in Bryan et al. (2002) (grey star). A two-step liquid line of descent (LLOD) is plotted, starting from a primitive DHF basanite (14 wt.% MgO) and the DHF tephrite from Bryan et al. (2002). The LLOD was computed using rhyolite-MELTS (Gualda et al., 2012), simulating fractional crystallization at isobaric conditions (400 MPa) and initial H_2O of 1.5 wt%). Mineral-melt partition coefficients for V, Ba and Zr in olivine, clinopyroxene, plagioclase and alkali feldspar were taken from Larsen (1979), Vilemant et al. (1981), Bindeman et al. (1998) and Adam and Green (2006). In this diagram, pure mixing trends would occupy the lower part of the diagram, with little or no influence of alkali feldspar cumulate melting. Addition of a component of cumulate melting results in a shift towards the upper, Ba-rich zone of the diagram (dashed black line, numbers mark vol.% of added *kfs*), notably above the LLOD. In this scheme, banded pumices would represent mixing and melting of low-Zr felsic cumulate, while mafic scoriae plot well below the LLOD and represent mixing of the tephritic end-member with an array of phonolitic compositions from high-Zr to low-Zr. Symbols as in **Fig. 6**.

Fig. 15. Sketch of the plumbing system leading to the caldera-forming eruption of El Abrigo at ca. 170 ka (a). In this view, protracted storage in a lower crustal reservoir produced a tephrite from fractional crystallization of basanite, which was periodically replenished (b). Upon ascent, the tephritic magma encountered the zoned, shallow phonolitic reservoir, sequentially interacting with a crystal-rich, low-Zr reservoir and a high-Zr, low crystallinity region (c), producing the observed distribution of trace elements. Sketch not to scale.

Fig. 1.

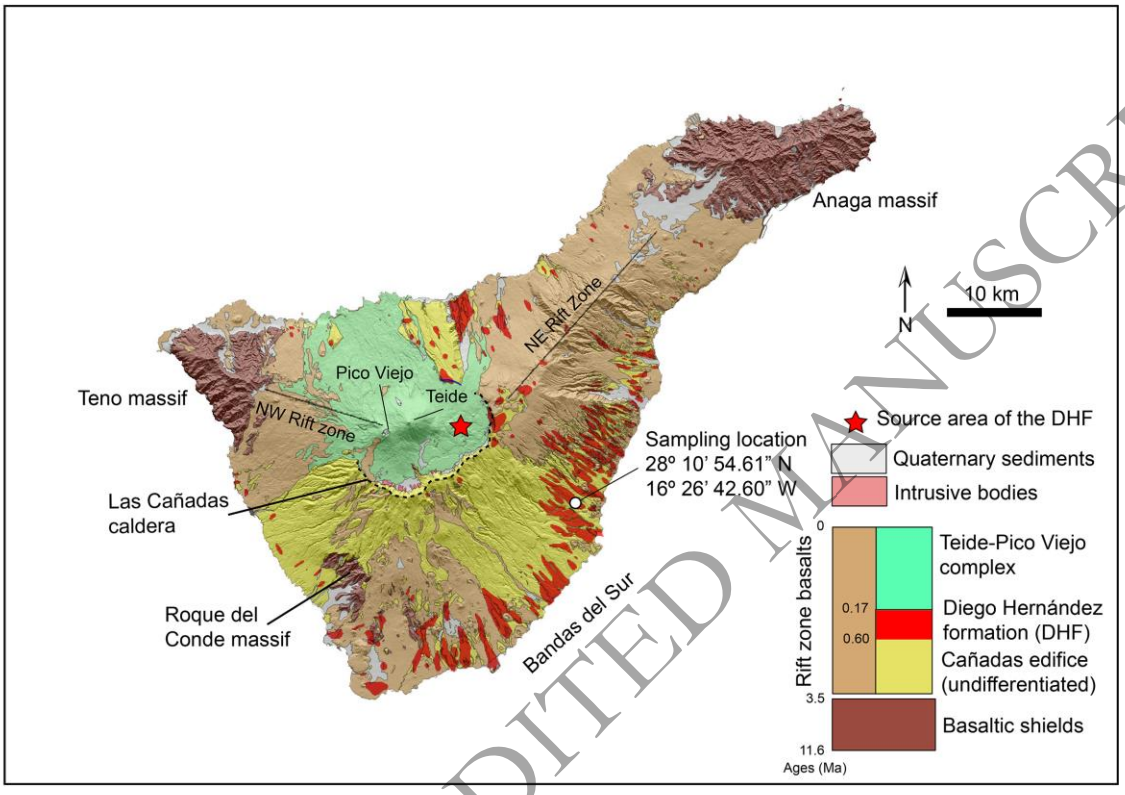

Fig. 2.

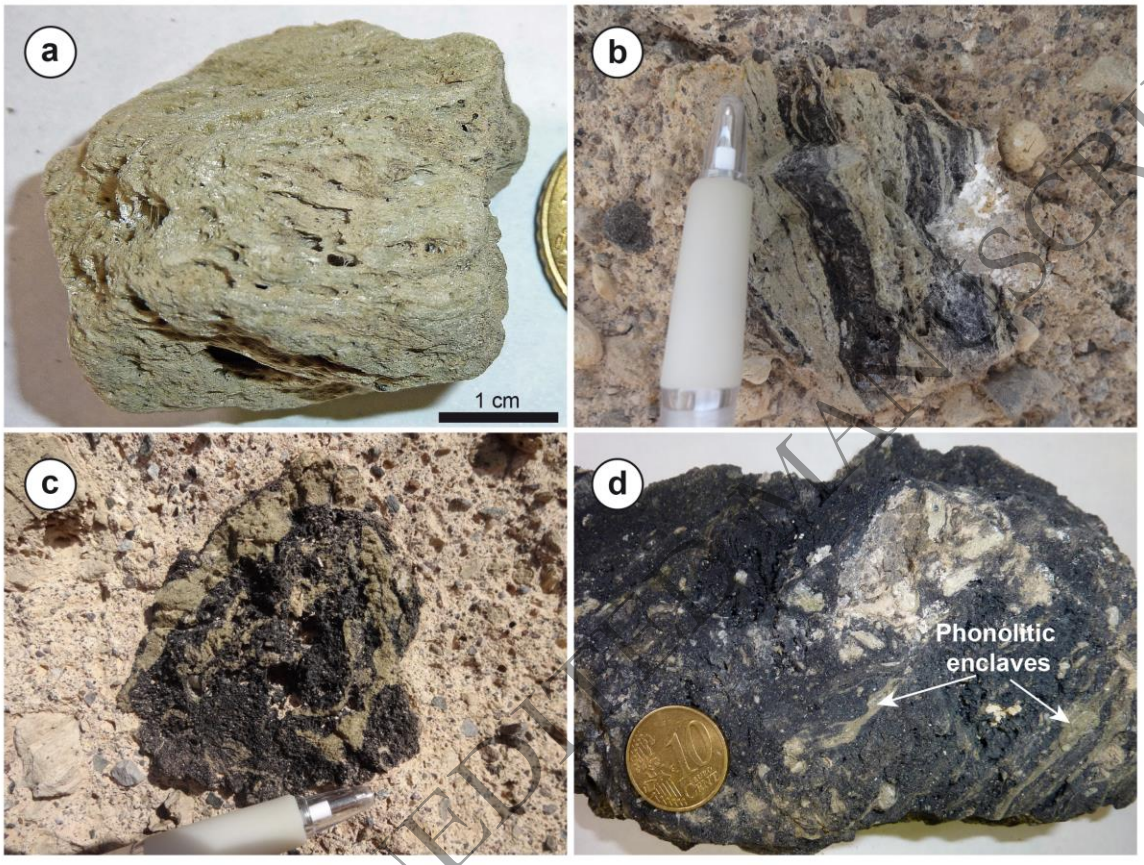

Fig. 3.

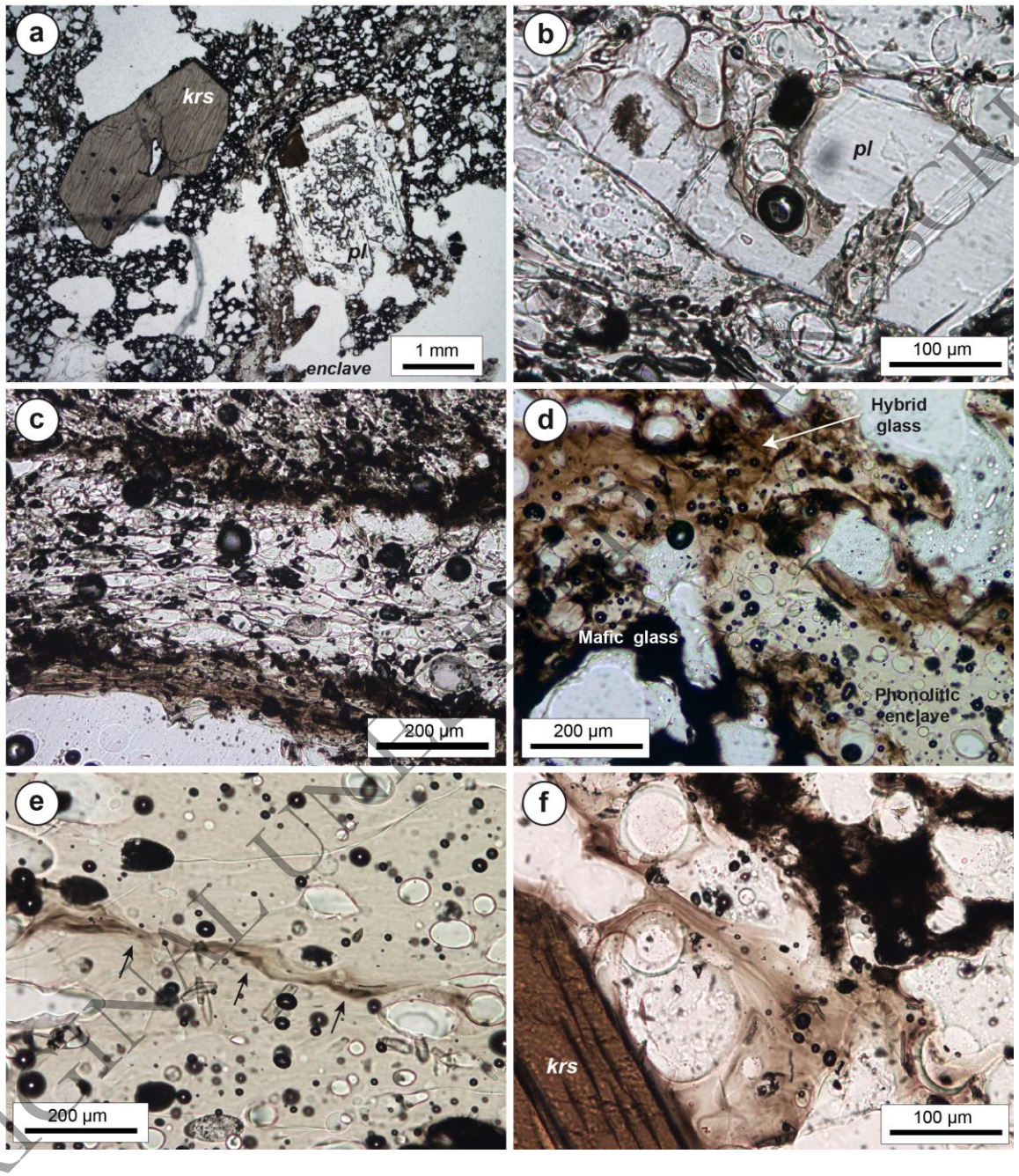

Fig. 4.

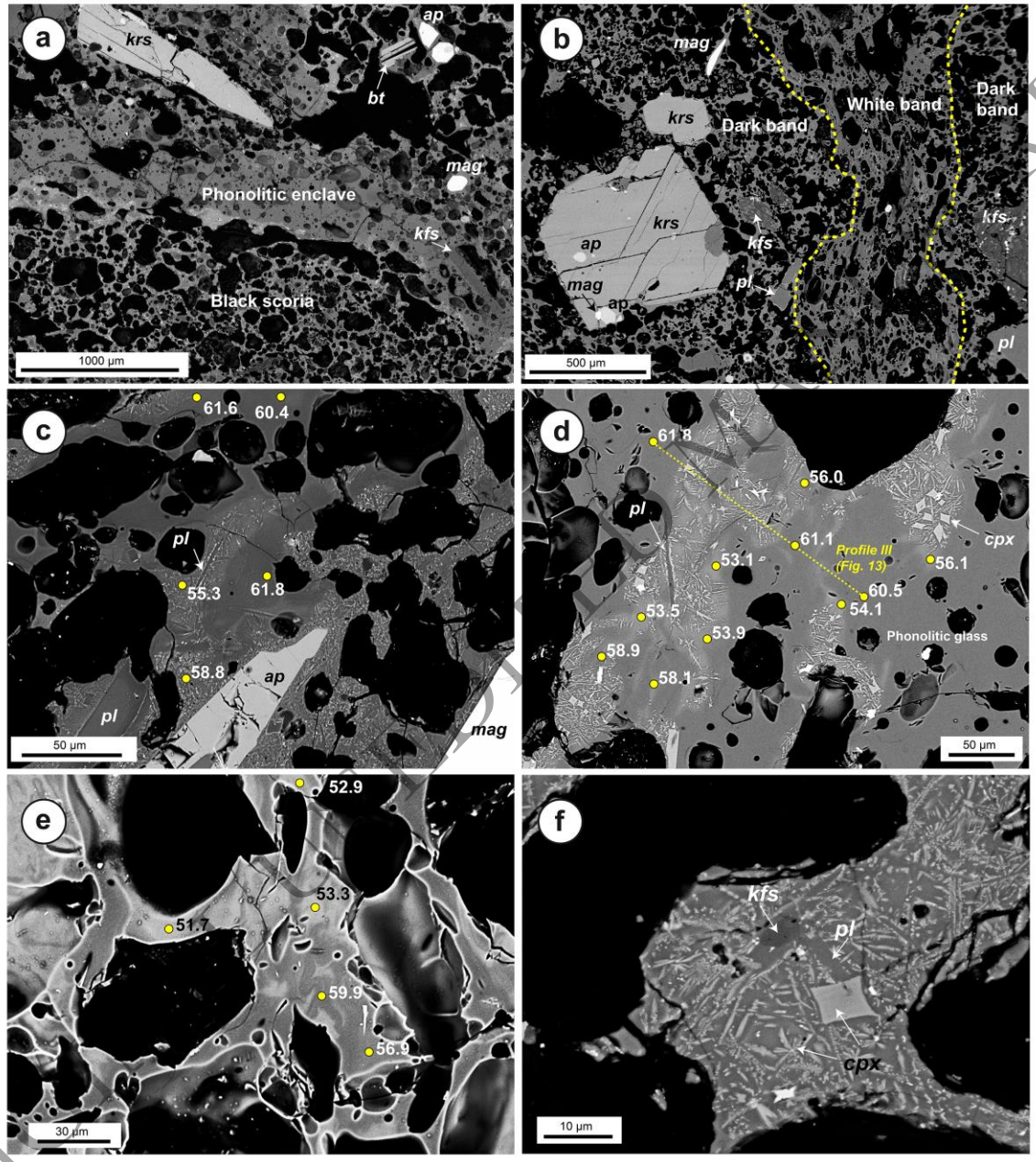

Fig. 5.

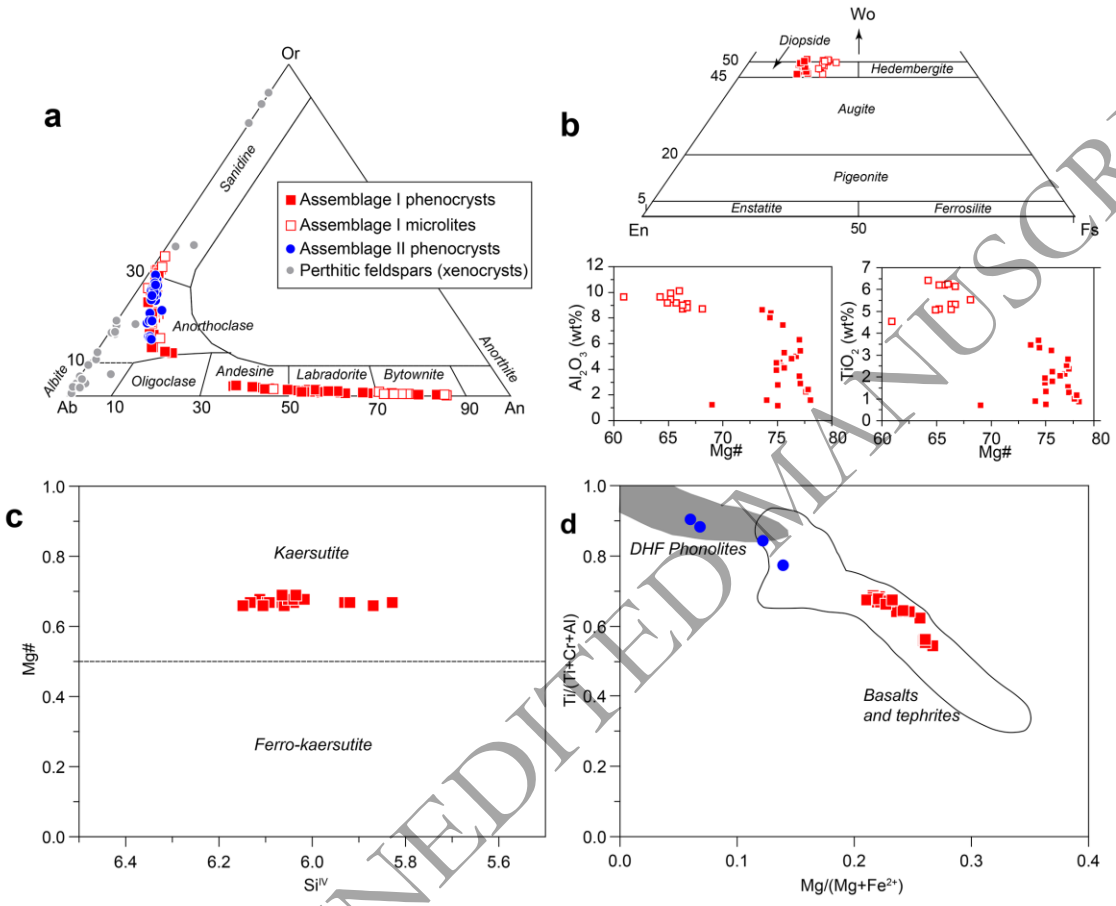

Fig. 6.

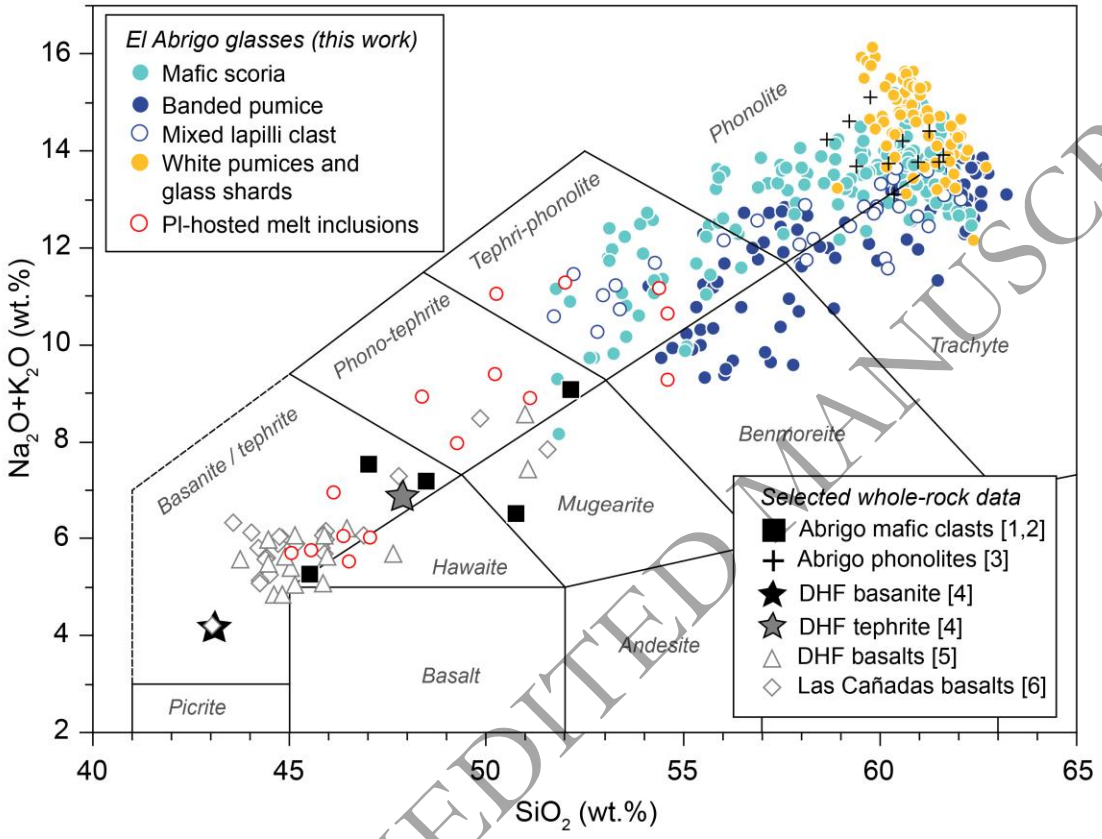

Fig. 7.

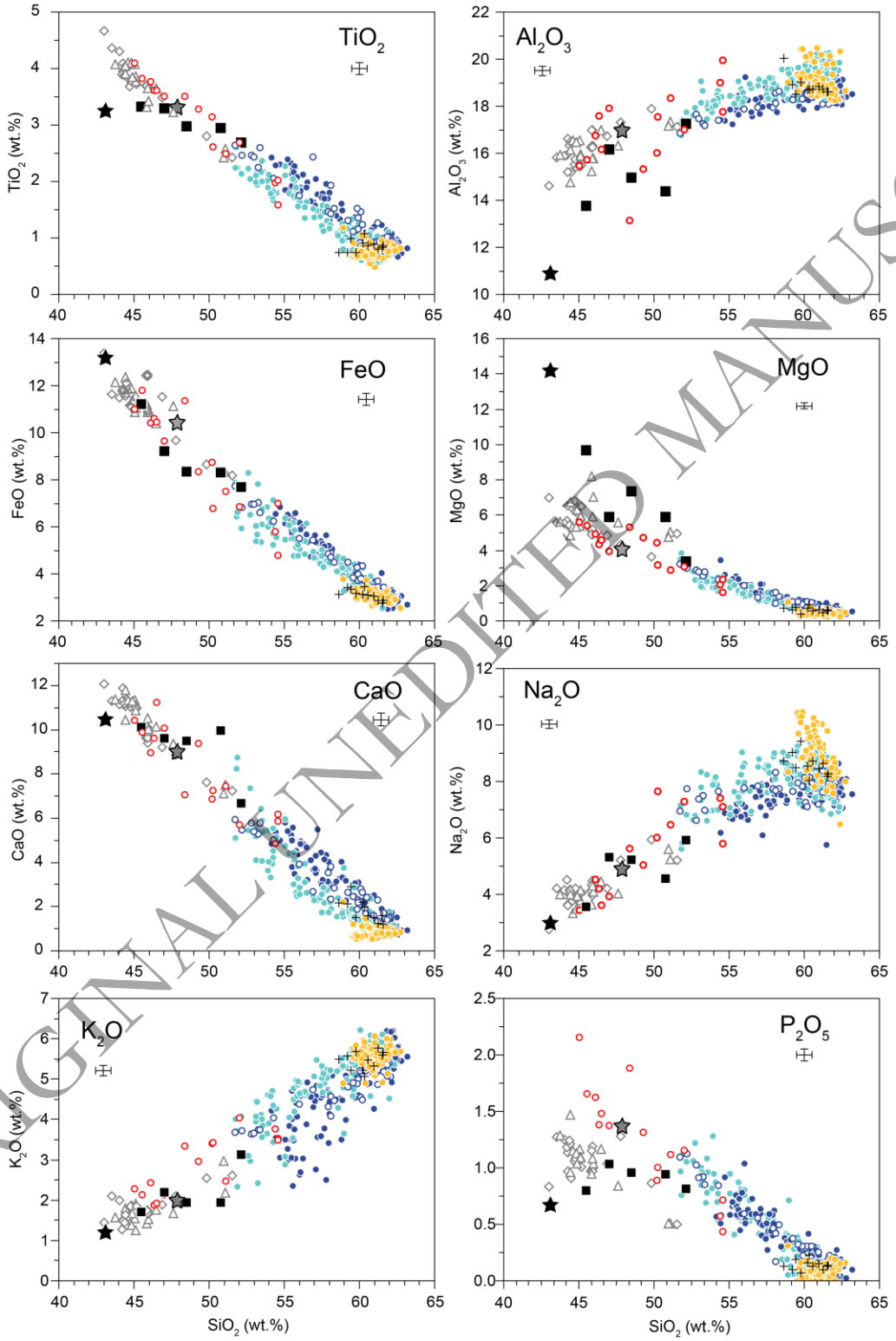

Fig. 8.

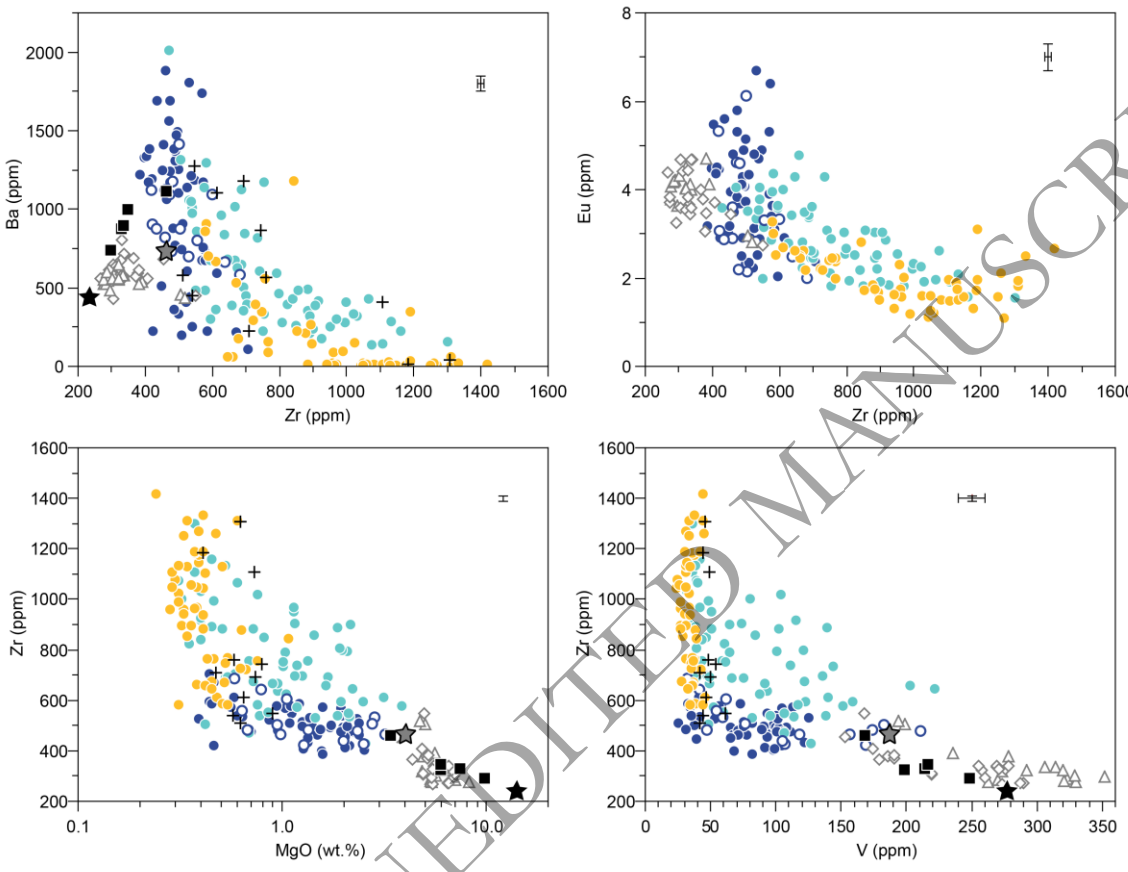

Fig. 9.

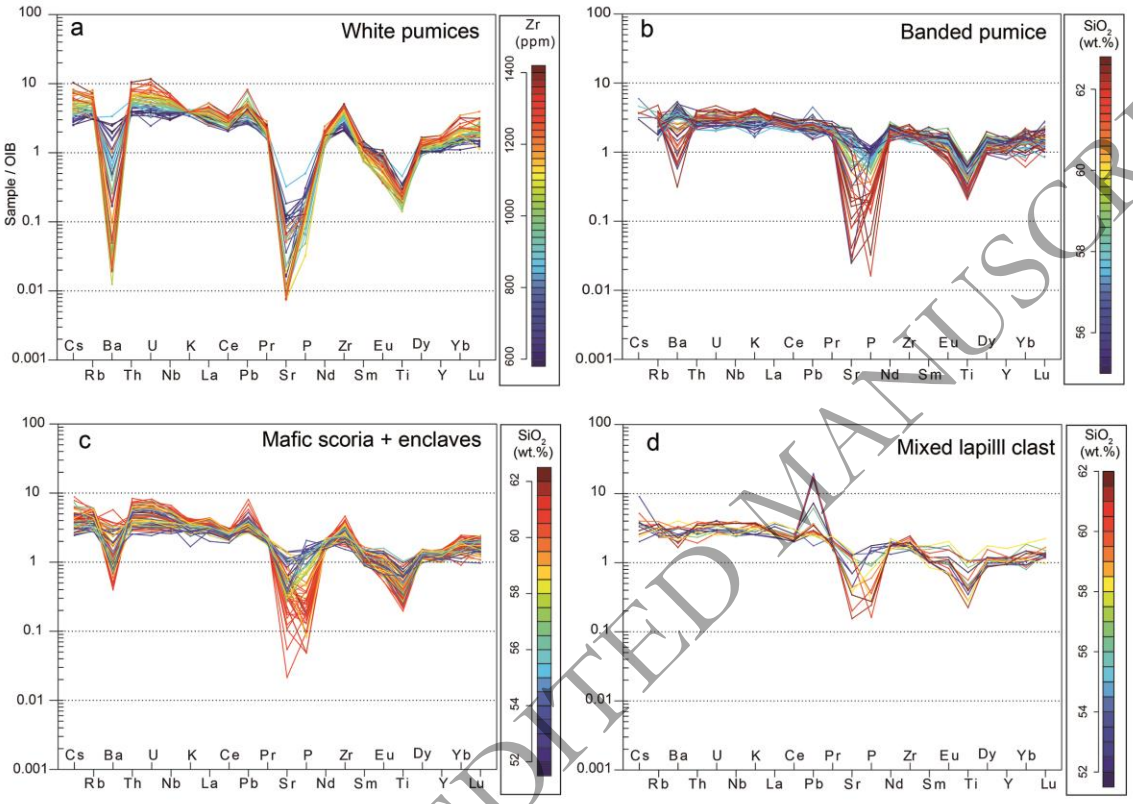

Fig. 10.

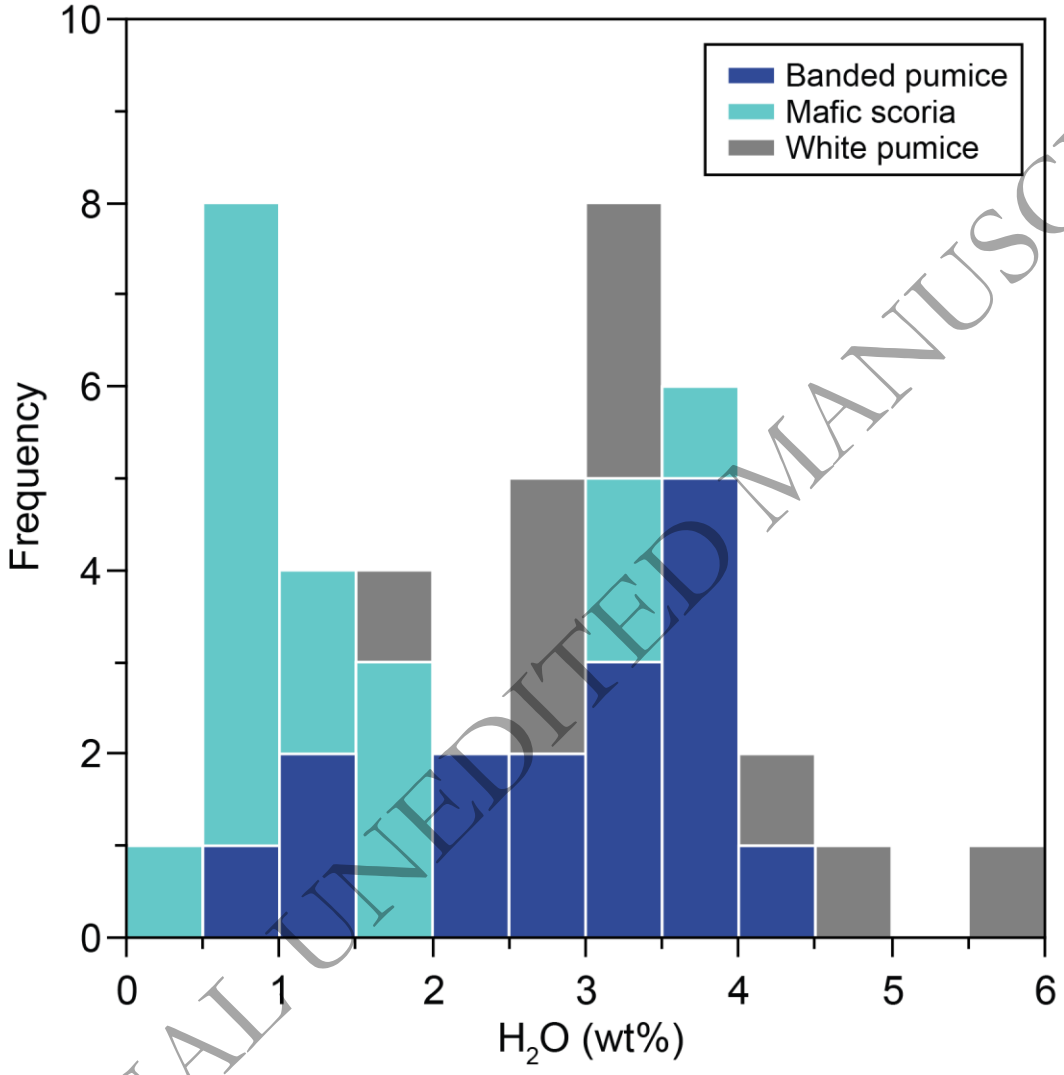

Fig, 11.

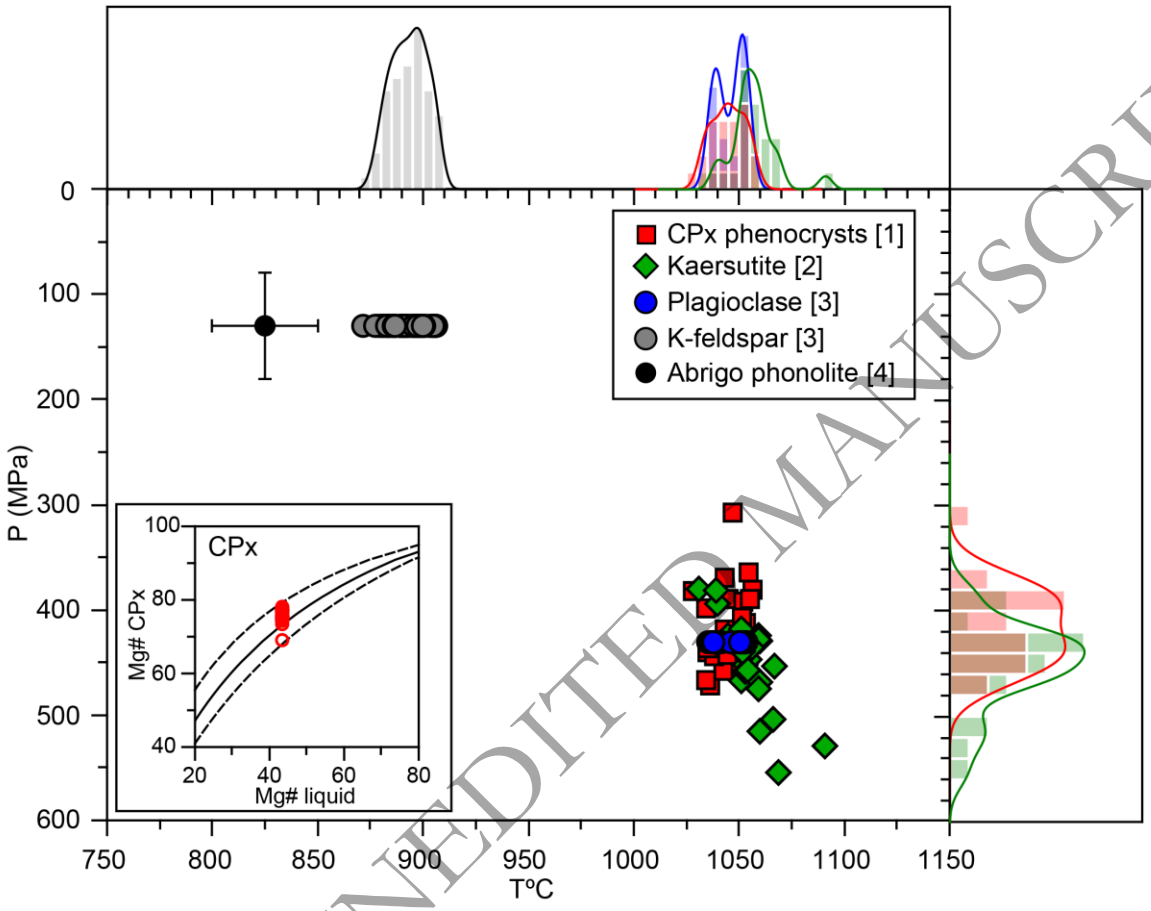

Fig. 12.

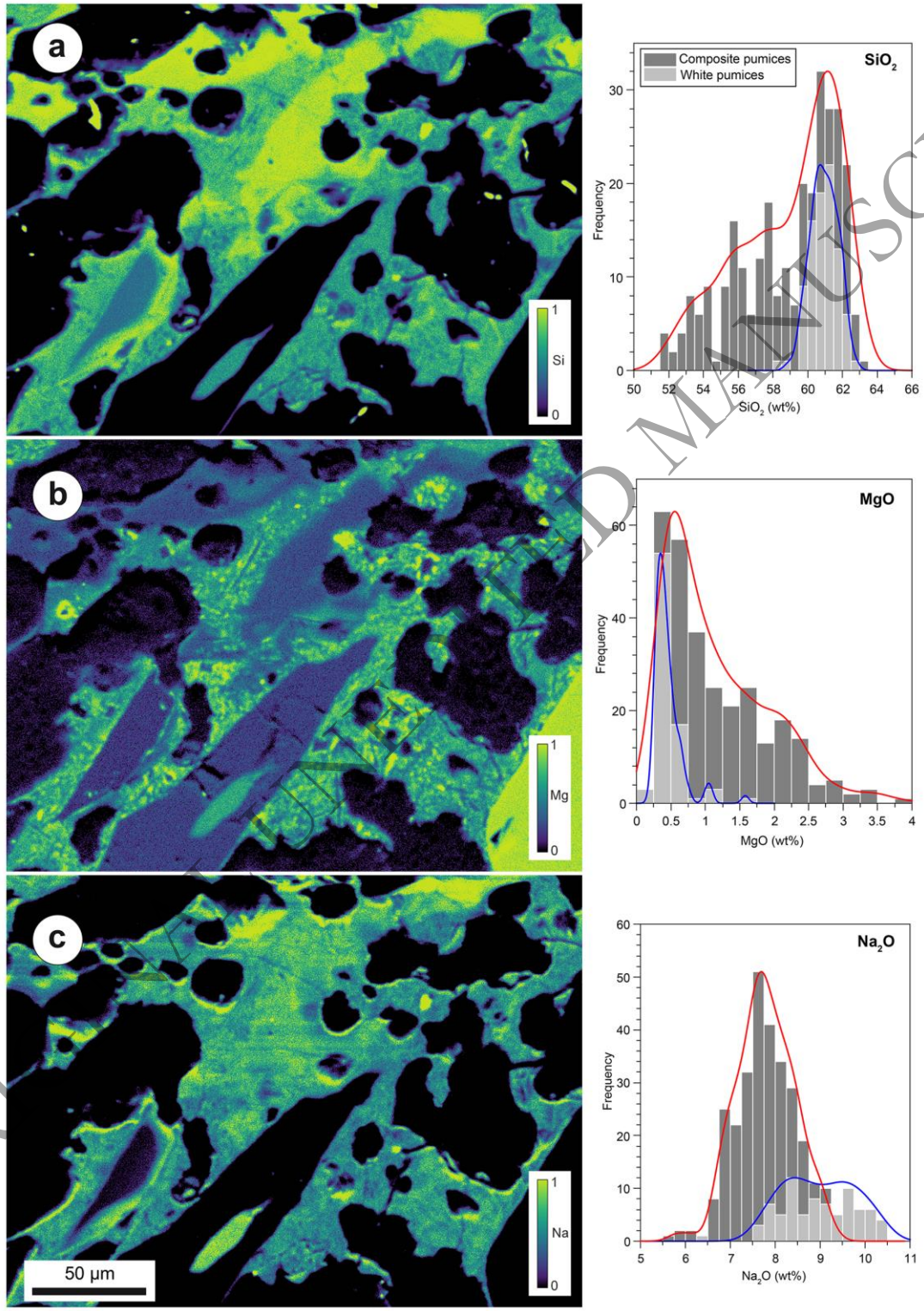

Fig. 13.

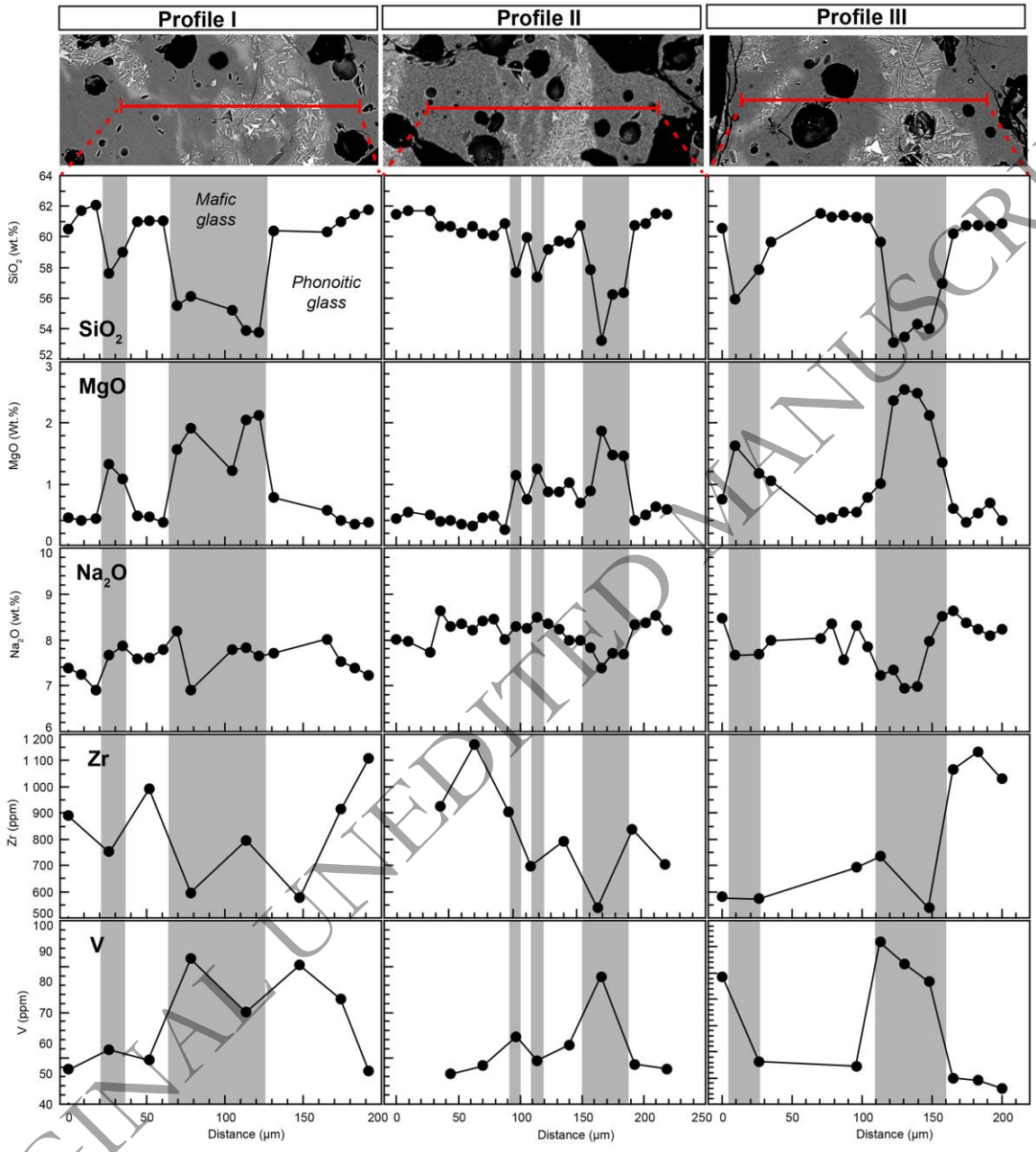

Fig. 14.

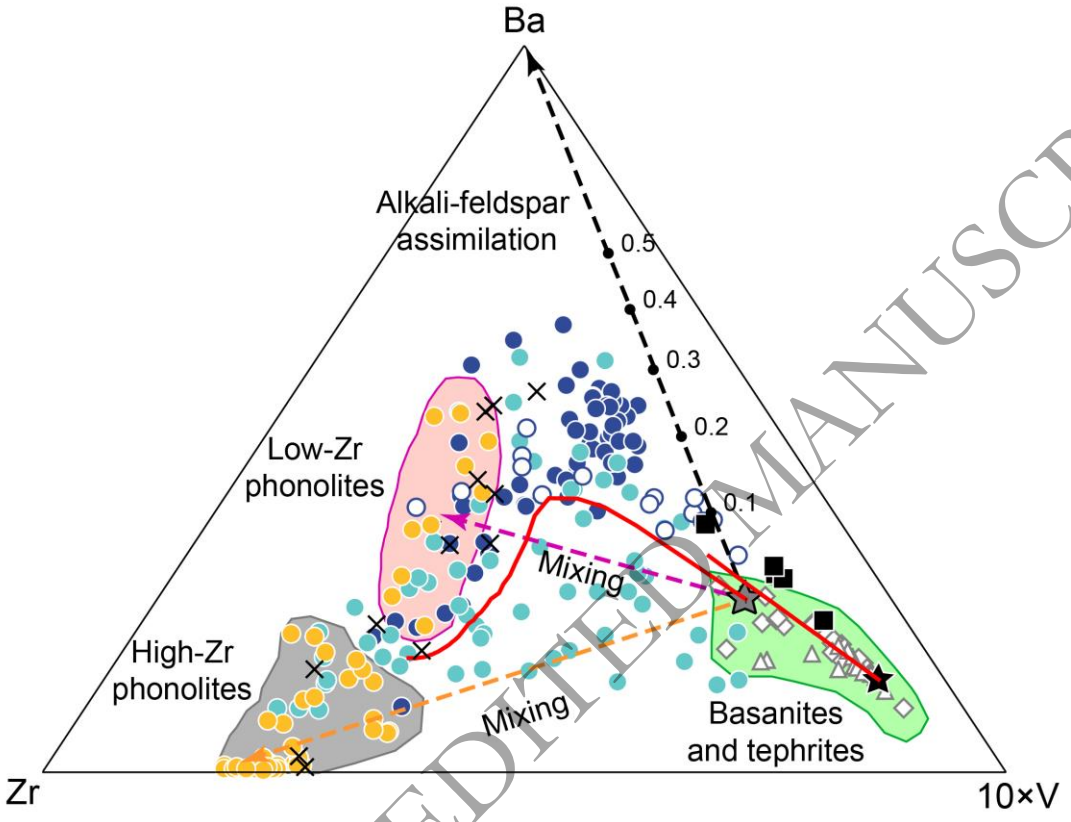

Fig. 15.

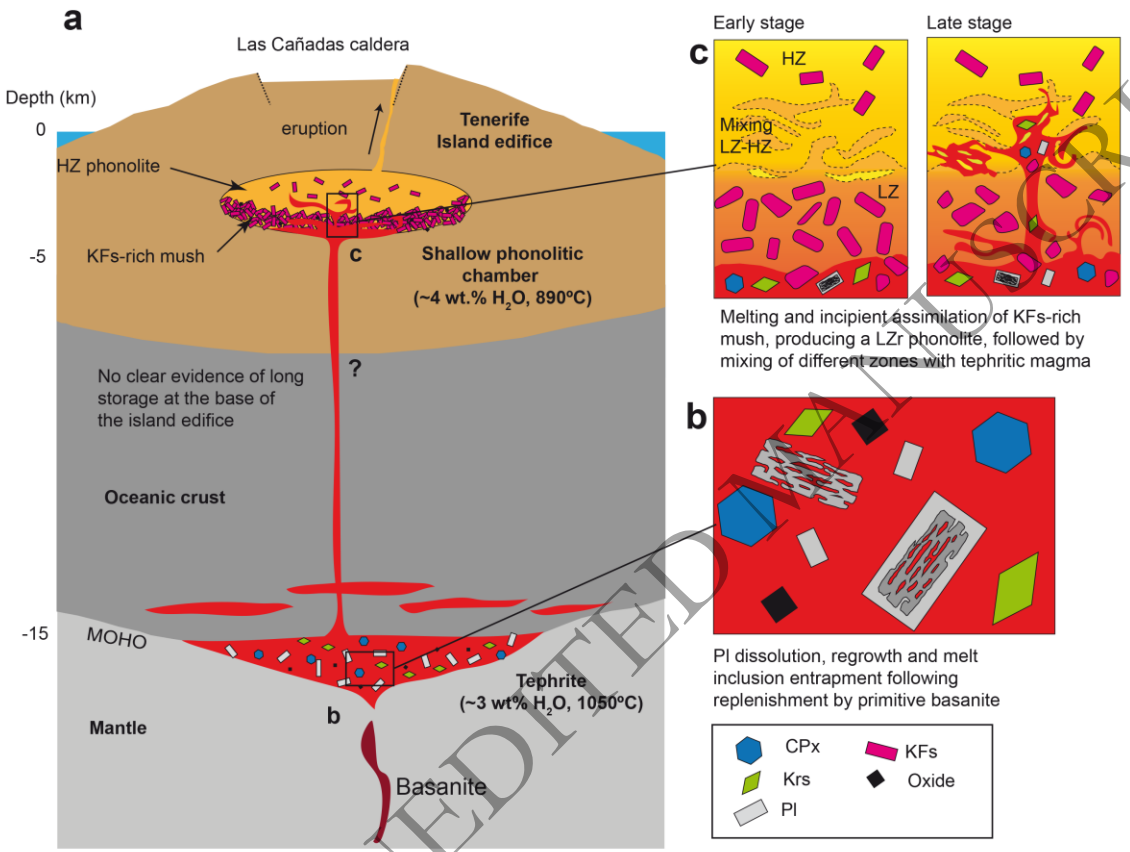

Table 1. Summary of petrographic features

Type	Samples	Zonation	Glass	Mineral content	Notes
Lapilli tuff	ABP-F1, F2	Lithics	Present in some lithics	Varied	Igneous, from mafic to felsic. Some of them have a glassy groundmass
		Pumices	Phonolitic to phono-tephritic	Very scarce (*mag, ttn*)	Juvenile, mixed to felsic. See below
		Free minerals	-	*kfs*, *pl*, minor *hau*	
		Ashy matrix	Phonolitic	-	Glass shards
			JUVENILE CLASTS		
White pumices	ABP-F5, F6	-	Phonolitic	Aphyric	Glass only, highly vesicular
Black scoriae with white enclaves	ABP-M	Mafic scoria	Phono-tephritic, mixed	Assemblage I (*pl, kfs, krs, cpx, bt, ap, mag*)	Medium vesicularity, partially crystallized.
		White enclaves	Phonolitic, mixed	Assemblage II (*kfs*)	Prominent mixing features
Banded pumices	ABP-C	Dark bands	Phono-tephritic, mixed	Assemblage I (*pl, kfs, krs, cpx, bt, mag, ilm, ap*)	Porphyritic, medium vesiculatiry. Mafic portion is finely crsytallized
		White bands	Phonolitic	Assemblage II (kfs, bt, mag, ap)	*kfs* phenocrysts, highly vesicular, anisotropic

Mineral abbreviations: *cpx* = clinopyroxene; *krs* = kaersutite; *pl* =plagioclase; *kfs* = alkali feldspar; *bt* = biotite; *ap* = apatite; *mag* = magnetite; *ilm* = ilmenite; *ttn* = titanite; *hau* = haüyne

Table 2. Summary of thermobarometric calculations

Method	Reference	*n*	P (MPa)	T (ºC)	SiO_2 in melt (wt.%)	H_2O (wt.%)	Comments
Amphibole	Ridolfi & Renzulli (2012)	17	451 ± 43	1056 ± 12	51.2 ± 2.2**	2.9 ± 0.5	Kaersutites
CPx-melt	Masotta et al. (2012)	22	412 ± 38	1044 ± 8	*51.1**	*3**	Phenocrsyts + PT51 glass
Plagioclase-melt	Putirka (2008)	20	*431**	1044 ± 7	*51.1**	*3**	Labradorite and bytownite + PT51 glass
Plagioclase hygrometry	Waters & Lange (2015)	20	*431**	*1044**	*51.1**	*1.8-2.2*	Labradorite and bytownite
Alkali feldspar-melt	Putirka (2008); Mollo et al. (2015)	25	*130**	893 ± 9	*59.9**	4.1 ± 1.1	Kfs phenocryst + HZr phonolite

n = number of mineral analyses or mineral-melt pairs used
* Values used as input in the corresponding model. In alkali feldspar thermometry, the P value is from Andújar et al. (2008)
** SiO_2 in melt in amphibole thermobarometry is calibrated only for calk-alkaline melts, hence it should be taken as indicative only